Implications of the Inflation Reduction Act on Deployment of Low-Carbon Ammonia Technologies

Chi Kong Chyong[a,b], Eduardo Italiani[a], Nikolaos Kazantzis[c]

[a] *Center on Global Energy Policy, School of International and Public Affairs, Columbia University*
[b] *Center for Energy and Environmental Policy Research, MIT*
[c] *Department of Chemical Engineering, Worcester Polytechnic Institute*
Corresponding author: kc3634@columbia.edu

Supplementary Information

Table of Contents

A. Technical Foundation of the Techno-Economic Analysis

The technical underpinnings of the proposed techno-economic performance assessment framework are associated with a fixed-scale configuration of various integrated process units found in the pertinent literature as various process units illustrated below (Figure A-1).

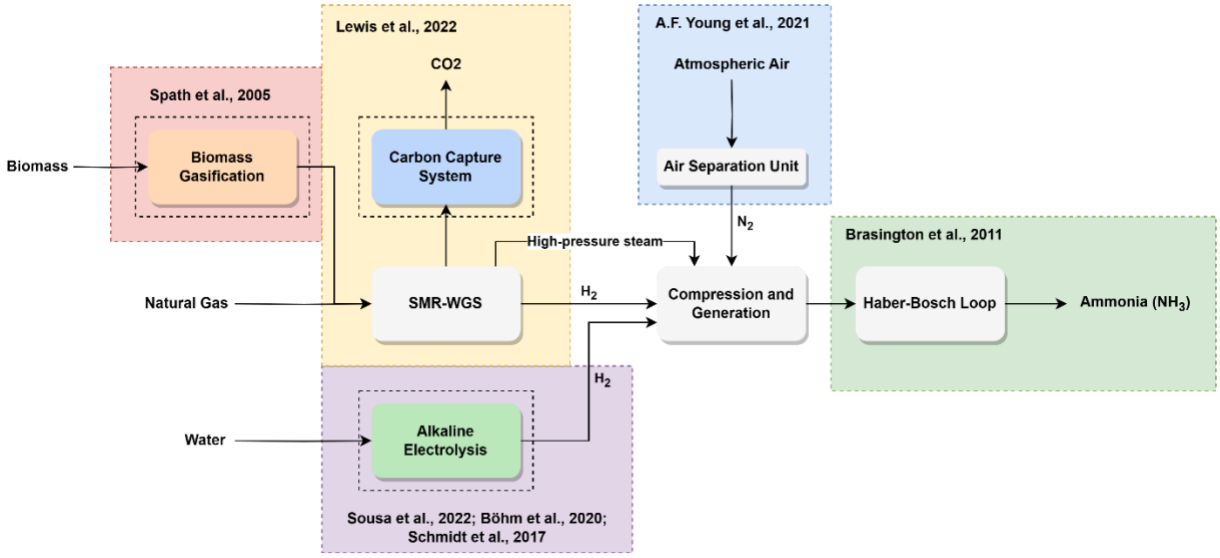

Figure A-1: Simplified illustration of the structure of a composite technical process system model.

The design concept underlying the ammonia process system under consideration is aligned with the well-known Linde Ammonia Concept (LAC) (Amhamed et al., 2022). The advantage of this process design (as opposed to the Kellog-Braun approach) is that the air separation unit is separate from the SMR process, reducing the capacity requirements of the SMR equipment and thus reducing the overall cost. LAC is also easy to simulate as each process block/unit can be treated isolated.

The rest of this section is dedicated to explaining how we combined these process blocks/units in an integrated process system configuration and formed the requisite technical foundations of this study.

Table A-1: Nomenclature in this SI A.

Variable	Description	Units
η_{AEC}	Electrolysis efficiency, LHV basis	H2 LHV
$h_{H_2}^{LHV}$	Hydrogen LHV	kWh/kg
M_{H_2}	Hydrogen production flowrate	Tonnes per day (TPD)
M_{NH_3}	Ammonia production flowrate	TPD
R_{CO_2}	CCS CO2 Capture rate	w%/w%
h_{NG}^{LHV}	Natural gas LHV	MJ/kg
$M_{biomass}$	Mass flowrate of biomass	TPD
$Y_{biomass}$	Kg of hydrogen per tonne of biomass	Kg H2/tonne biomass

$\dot{M}_{NG_j}$	Energy flowrate of natural gas for technology j	MMbtu/year

A.1. AP SMR and AP CCS

The hydrogen production details were based on NETL's economic analysis reports, particularly Case 1, involving a conventional SMR option, and Case 2, associated with conventional SMR with an integrated CCS system (Lewis et al., 2022). For large-scale production of N2, cryogenic distillation is preferred. The process for the ASU was also obtained from (A. F. Young et al., 2021). Finally, the ammonia synthesis loop came from NETL's report by Bransington et al., particularly Case 4, stream 38 (Brasington et al., 2011).

Table A-2 contains all relevant inlet and outlet streams of the three LAC production blocks necessary for the design of the multi-stage compression. The resulting scale is 2717 TPD of NH3, assuming a nitrogen conversion of 99.9% through HB (Brasington et al., 2011). The ASU study scale was increased by 6.15% (2100 TPD to 2237 TPD) to match hydrogen production in a 3:1 H2/N2 (H2 flowrate in Table A-2) molar ratio (Lewis et al., 2022; A. F. Young et al., 2021).

The PFD, mass, and energy information of the multi-stage compression and cooling used to integrate the SMR-WGS hydrogen and the ASU nitrogen into the Haber-Bosch loop and electricity generation from surplus steam can be found in Figure A-2 and Table A-4. All compressors are modeled as isentropic. The steam turbine was assumed to have an isentropic efficiency of 72% and the make-up compressors 85%, while the resulting work was more than 50MW. The latter is an overestimate compared to IEAGHG's report on SMR AP; hence, we assume a generation of 25MW, which closely resembles the results in the IEAGHG report (IEAGHG, 2017).

AP CCS and AP AEC will not include the CAPEX of the steam turbine as surplus steam is not generated. AP SMR and AP BH2S will include the steam turbine. See the attached Excel file with the equipment list called ***AP_NE_Equipment_List.xlsx***.

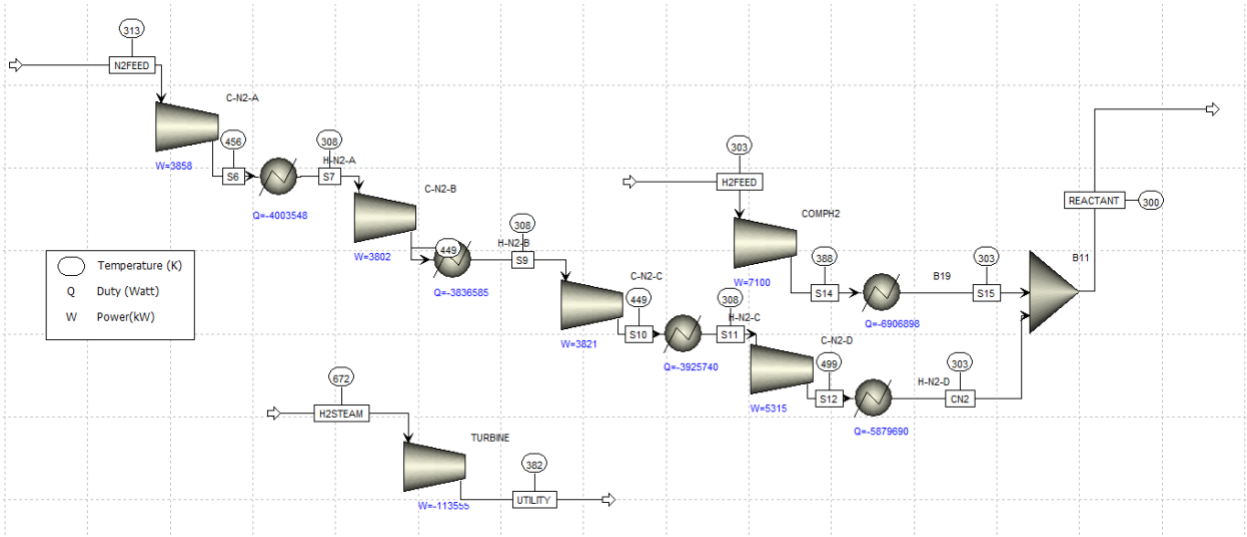

Figure A-2: Compression system for AP CCS, AP BH2S, and AP SMR. AP CCS does not generate electricity.

Table A-2: Inlet and outlet streams of selected literature processes

	H2 Outlet (Lewis et al., 2022)	**N2 Outlet** (A. F. Young et al., 2021)	**Surplus Steam from H2** [a](Lewis et al., 2022)	**Ammonia Synthesis Reactant Inlet** (Brasington et al., 2011)
Flowrate [TPD]	483.02	2,100.4	18,617.0	2,632.9
Temperature [C]	30	40	399	21
Pressure [MPa]	6.48	0.0980	3.1	13.614
Vapor Fraction	1	1	1	1
H_2 [mol/mol]	0.9998	0.0000	0.0000	0.7490
N_2 [mol/mol]	0.0002	1.0000	0.0000	0.2500
H_20	0.0000	0.0000	1.0000	0.0000
O_2	0.0000	243 ppb	0.0000	0.0000
Ar	0.0000	18 ppm	0.0000	0.0010
Total	1.0000	1.0000	1.0000	1.0000

[a] Surplus steam is only available for conventional SMR. In SMR CCS, the surplus steam is used to heat the amine regenerator (Lewis et al., 2022).
[b] Oxygen and Argon are neglected from this study's mass balance because these species are within specification, and their effects on HB catalyst deactivation are accounted for through the variable O&M from (Brasington et al., 2011).

A.2. AP BH2S

The AP BH2S unit was obtained from (Spath et al., 2005) and was combined with the inlet of the SMR-WGS hydrogen production process. Specifically, stream 327 of the current design for BH2S was combined with stream 3 of Case 1 of Lewis et al. (Lewis et al., 2022; Spath et al., 2005). Table A-3 includes the difference in the stream compositions before entering the SMR reactor. The SMR reactors for both studies are modeled as equilibrium reactors with similar

design parameters (S/C ratio, pressure, and temperature) (Lewis et al., 2022; Spath et al., 2005). Hence, for the BH2S scenario, we assume that the SMR outlet composition, temperature, and pressure differences are negligible for this techno-economic analysis. Given this assumption, we assume the process equipment before the SMR reactor comes from (Spath et al., 2005). After the SMR reactor, we assume the equipment from (Lewis et al., 2022) is used. To ascertain the amount of biomass required to fulfill the hydrogen production of the SMR process in (Lewis et al., 2022), we use the hydrogen yield from dry biomass by (Spath et al., 2005).

$$\dot{M}_{biomass} = \dot{M}_{H_2} * 1000 * \frac{1}{Y_{biomass}} \quad \text{(A.1)}$$

Table A-3: BH2S composition difference between (Lewis et al., 2022) and (Spath et al., 2005) at the SMR inlet.

Species	X_i AP	X_i AP BH2S
H2O	67.6%	40%
H2	4.3%	32%
CO	0%	19%
CO2	1.7%	8%
CH4	25.8%	1%

A.3. AP AEC

For the electrolysis system, the CAPEX and OPEX values were obtained from the literature (Böhm et al., 2020; Schmidt et al., 2017). A robust study by Sousa and colleagues estimated the outlet conditions of the electrolysis hydrogen stream – their values were used to model the inlet in the compression module (Sousa et al., 2022). We acknowledge that Sousa and colleagues prefer PEM, not AEC, as the technology option. Nevertheless, this assumption is appropriate. The outlet hydrogen stream out of PEM and AEC are found under similar conditions. Schmidt et al. (2017) indicate that AEC H2 outlet conditions are less than 30 bar and 60-80C. Sousa et al.'s H2 outlet conditions are 29 bar and 65C; therefore, this assumption holds (Sousa et al., 2022). Hence, the only difference between AEC and PEM using our modeling methodology would be the cost per kW of capacity, energy efficiency, and cell lifetime. We tune these parameters to AP AEC (see SI C).

The water content in the hydrogen stream is separated by a separator block on ASPEN and is cost-estimated as a cylindrical vertical vessel (2m diameter by 10m length) using the heuristics proposed by Turton et al. (2018) (see Excel file named ***AP_NE_Equipment_List.xlsx***).

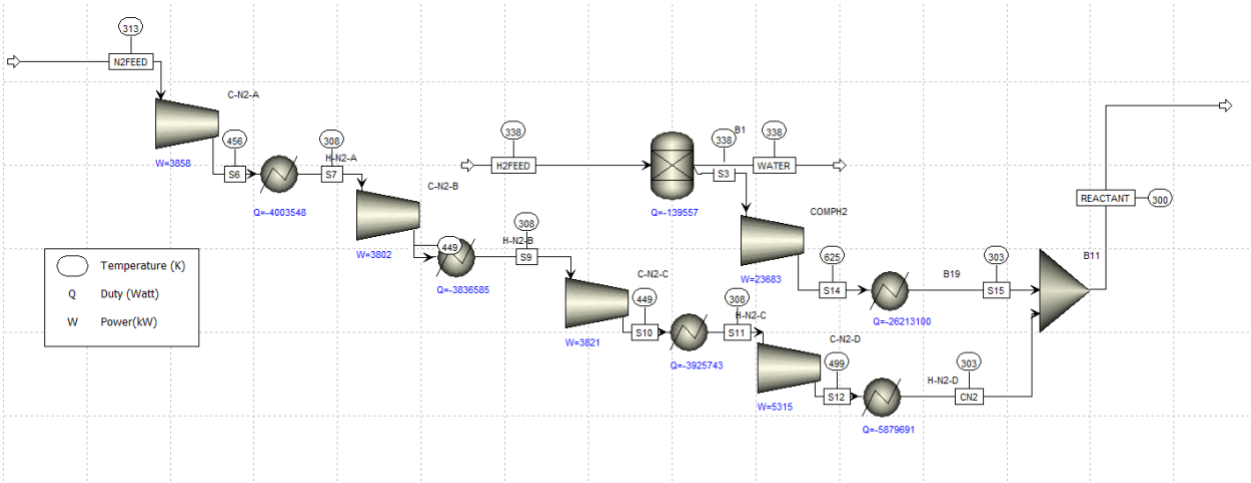

Figure A-3: Compression system for AP AEC.

Table A-4: Stream information for make-up compression and steam turbine for AP SMR, AP CCS, and AP BH2S.

	H2FEED	N2FEED	REACTANT	STEAM IN	STEAM OUT	NH3_OUT
Flowrate [TPD]	483.0	2237.0	2720.0	18617.0	18617.0	2717
Flowrate [kmol/hr]	9958.0	3327.3	13285.3	43058.4	43058.4	6647.4
Temperature [C]	30	40	26.5949	399	109.3491	21
Pressure [MPa]	6.48	0.098	13.614	3.1	0.1	13.614
Vapor Fraction	1	1	1	1	1	1
H_2 [mol/mol]	1.000	0.000	0.749	0.000	0.000	0.000
N_2 [mol/mol]	0.000	1.000	0.251	0.000	0.000	0.000
H_20 [mol/mol]	0.000	0.000	0.000	1.000	1.000	0.000
O_2 [mol/mol]	0.000	0.000	0.000	0.000	0.000	0.000
Ar [mol/mol]	0.000	0.000	0.000	0.000	0.000	0.000
Nh3 [mol/mol]	0.000	0.000	0.000	0.000	0.000	1.000
Total	1.000	1.000	1.000	1.000	1.000	1.000

A.4. Utility, feedstock, and product flowrates and miscellaneous technical variables.

Table A-5: Key technical parameters.

Input Name	Value	Unit	Source
$\dot{M}_{NH_3}$	2717	TPD	Calculated assuming 99.9% conversion of N_2
$\dot{M}_{H_2}$	483.013	TPD	Lewis et al. 2022

η_{AEC}	uniform(70%, 78%)	TPD	Brauns et al., 2020
$h_{H_2}^{LHV}$	33.3333	kWh/kg	
R_{CO2}	95.6%	W%/w%	Lewis et al., 2022
h_{NG}^{LHV}	47.1	MJ/kg	Engineering Tool Box, 2003
$Y_{biomass}$	70.1	Kg H2/tonne biomass	Spath et al., 2005

Table A-6: Electricity requirements

Input Name	Value[A]	Unit	Source
AP SMR	HP: 13, AP: 64	MW	Lewis et al., 2022; Brasington et al., 2011; A.F. Young et al., 2021; Spath et al. 2005
AP CCS	HP: 41, AP: 117	MW	
AP BH2S	HP: 76.6, AP: 127	MW	
AP AEC	HP: $\frac{\dot{M}_{H_2} \times h_{H_2}^{LHV} \times 1000}{\eta_{AEC}}$, AP: $\frac{\dot{M}_{H_2} \times h_{H_2}^{LHV} \times 1000}{\eta_{AEC}} + 52$	MW	Lewis et al., 2022; Brasington et al., 2011; A.F. Young et al., 2021; Böhm et al., 2020.

[A] HP stands for hydrogen production and shows the electricity demand for hydrogen production. AP is hydrogen production plus the electricity demand from HB, ASU, and the compression system.

Table A-7: Natural gas requirements, $\dot{M}_{NG_j}$

Input Name	Value[A]	Unit	Source
AP SMR	25039232.02	MMBtu/yr	Lewis et al., 2022
AP CCS	26624225.74	MMBtu/yr	Lewis et al., 2022
AP BH2S	0	MMBtu/yr	Assumption
AP AEC	0	MMBtu/yr	Assumption

[A] The natural gas flowrates were directly obtained from case 1 and 2 of Lewis et al., 2022. Refer to stream number 3. We used the h_{NG}^{LHV} and the MMBtu conversion factor to convert to energy units.

Table A-8: Water demand

Input Name	Value	Unit	Source

AP SMR	52709532285	Kg/year	Lewis et al., 2022; Brasington et al., 2011; Young et al., 2021; Spath et al. 2005
AP CCS	54034044285	Kg/year	
AP BH2S	53448253002	Kg/year	
AP AEC Osmosis[A]	1332790200, 73077302619	Kg/year	Lewis et al., 2022; Brasington et al., 2011; Young et al., 2021; Sousa et al., 2022.

[A] The first value provided is the reverse osmosis flowrate. The second value is the process water demand. For more details on how the water demand was calculated, see the annexed Excel file called ***AP_NE_Water_Balance.xlsx***.

B. Techno-Economic Quantities of the Technical Process System Model

B.1. Objectives

This section aims to determine the equipment capacities for the AP process by combining the processes discussed in the previous section. These equipment capacities directly influence the capital expenditure ($\boldsymbol{CAPEX_j}$) associated with technology $\boldsymbol{j}$, where:

$$\boldsymbol{j} \in \{\boldsymbol{AP\ SMR, AP\ CCS, AP\ BH2S, AP\ AEC}\} \quad \text{(B.1)}$$

Additionally, the demands for feedstock, utilities, and other raw materials can be obtained from the mass and energy balances from the reports. This will constitute the variable operating costs. The fixed operating costs, however, are estimated based on the number of unit operations required to operate the plant. These types of costs constitute the operational expenditure ($\boldsymbol{OPEX_j}$).

The goal of this section is to describe the methodology used to estimate the $\boldsymbol{CAPEX_j}$ and $\boldsymbol{OPEX_j}$ for each technology option, following the techno-economic approach outlined by Peters et al. (2003). These two quantities will allow for calculating the desired financial variables in ensuing sections (i.e., NPV, CAC, etc.).

Table B-1: Nomenclature for the CAPEX section.

Parameters	Description	Units
$\boldsymbol{j}$	Technology index	
$\boldsymbol{z}$	Cost factor index	

x_z	CAPEX cost factor	% EC_{u_j}
$CAPEX_j$	Capital Expenditure cost for technology j	$
$P_{(n_0,t_0,z)}$	Base capacity equipment cost.	$
m_n	number of spare equipment units required	$\mathbb{N}$
S_n	required equipment capacity	
S_{n0}	base capacity	
i	installation cost factor	
f	equipment economies of scale factor (Peters et al. 2003)	
C_{t_0}	Chemical engineering plant index at t_0	
C_{2023}	Chemical engineering plant index in 2023.	
M_{NG}	energy flowrate of natural gas	mmBTU/year
M_{EL}	electricity demand	kWh/year
$C_{EL}(T)$	electricity operating hour	hour
$CAPEX_{updated_j}$	updated CAPEX after adding the additional cost	$
FCI_J	Fixed capital investment of technology j	
EC_{u_j}	Uninstalled cost for technology j	$

EC_{i_j}	Installed cost for technology j	$
WC_j	Working Capital for technology j	$
$C_{I\&C}$	Cost factor for instrumentation and controls	% EC_{u_j}
C_p	Cost factor for piping	% EC_{u_j}
C_{el}	Cost factor for electrical	% EC_{u_j}
C_b	Cost factor for buildings	% EC_{u_j}
$C_{sf\&yi}$	Cost factor for service facilities and yard improvements	% EC_{u_j}
C_{land}	Cost factor for land	% EC_{u_j}
C_{eng}	Cost factor for engineering	% EC_{u_j}
C_L	Cost factor for legal	$
C_c	Cost factor for construction	% EC_{u_j}
C_{co}	Cost factor for contingency	% EC_{u_j}
C_{WC}	Cost factor for Working capital	% FCI
C_{AEC}	Cost of AEC electrolyzer	$/kWe

B.2. Model Formulation CAPEX

B.2.1. Estimating CAPEX

$$CAPEX_j = \sum_{z=0}^{z} [s_f \times x_z] \times \left[EC_{u_j}\right] + EC_{i_j} + C_{land} + WC_j \quad \text{(B.2)}$$

(B.2) describes how the $CAPEX_j$ was estimated. This method obtains the installed (EC_{i_j}) and uninstalled (EC_{u_j}) costs for a specific technology and calculates the $CAPEX_j$. The values for

EC_{i_j} and EC_{u_j} were calculated based on the equipment data sets described in section A. x_z is a cost factor for a set of facilities, z (Peters et al., 2003). C_{land} is the cost of land and a constant for all technologies. WC_j is the working capital (calculated in (B.4)).

The average value of the cost factors for each technology for each scenario is in annexed excel file named ***AP_NE_CAPEX.xlsx***. More detailed information on the CAPEX estimation methodology is in Peters et al. 2003. For clarity, we specify the cost factors below.

$$x_z \in \{C_{I\&C}, C_p, C_{el}, C_b, C_{sf\&yi}, C_{eng}, C_L, C_c, C_{co}\} \quad \text{(B.3)}$$

where each cost factor, C_z, corresponds to instrumentation and control, piping, electrical, buildings, service facilities and yard improvements, engineering, legal, construction, and contingency, respectively.

The working capital, WC_j, was calculated using the formula below (B.4).

$$WC_j = FCI_j * C_{WC} = \left(\sum_{z=0}^{z} [s_f \times x_z] \times \left[EC_{u_j}\right] + EC_{i_j} + C_{land}\right) \times C_{WC} \quad \text{(B.4)}$$

The textbook cost factors used to calculate $CAPEX_j$ and related parameters are based on a scale of the order of 100 TPD (Peters et al., 2003). Hence, each parameter was scaled by using the six-tenths rule to the AP scale of M_{NH_3} (2717 TPD NH3). The factor is defined as s_f.

$$s_f = \frac{1}{\left(\frac{100}{M_{NH_3}}\right)^{0.6}} \quad \text{(B.5)}$$

EC_{u_j} and EC_{i_j} were calculated using equations (B.6) and (B.7).

$$EC_{u_j} = \sum_{n=0}^{N} m_n * P_{(n,t_0,j)} * \left(\frac{S_n}{S_{n0}}\right)^f * \left(\frac{C_{2023}}{C_{t_0}}\right) \quad \text{(B.6)}$$

$$EC_{i_j} = \sum_{n}^{N} m_n * P_{(n_0,t_0,j)} * \left(\frac{S_n}{S_{n0}}\right)^f * (1+i) * \left(\frac{C_{2023}}{C_{t_0}}\right) \quad \text{(B.7)}$$

EC_{u_j} and EC_{i_j} are functions of the sum of the base-capacity uninstalled equipment costs $P_{(n_0,t_0,z)}$ where n_0 denotes the name of the piece of equipment (see equipment list, N, in Excel file named ***AP_NE_Equipment_List.xlsx***)[1], and t_0 is the time when the equipment cost was estimated. S_n is the required capacity of the piece of equipment. S_{n0} is the base equipment capacity. f are the economies of scale factor obtained from Peters et al. (2003) (also in the Excel file). $(1+i)$ is the installation factor obtained from Peters et al. (2003). C_{2023} is the

[1] The equipment list Excel file also contains the full calculations of EC_{u_j} and EC_{i_j}.

chemical engineering plant index (CEPCI) in 2023 and C_{t_0} is the CEPCI at the time the piece of equipment was cost estimated. m_n is the number of spares for a given piece of equipment ($m_n \in \mathbb{N}$).

B.2.2. Back-propagation of additional CAPEX on other CAPEX-related cost factors.

There are times when we need to add the cost of certain modules directly into the $CAPEX_j$ from the scientific literature. Once we do this, we also need to scale the cost components of the capex ($[s_f \times x_z] \times \left[EC_{u_j}\right]_.$) to be adjusted to the higher CAPEX. We perform the method described below for the AP AEC electrolyzer, wind farm, and battery storage costs[2].

We define a new variable R_j to represent the scaling ratio by which to increase each capex component.

$$R_j = 1 + \frac{C_{additional_j}}{CAPEX_{Updated_j}} \tag{B.8}$$

$$\left|[s_f \times x_z] \times \left[EC_{u_j}\right]_.\right|_{updated} = [s_f \times x_z] \times \left[EC_{u_j}\right]_. \times R_j \tag{B.9}$$

$CAPEX_{updated_j}$ is the updated CAPEX after adding the additional cost ($C_{additional_j}$). This ensures that the overall CAPEX estimate accurately reflects the depreciation effect of the additional costs on the project's financial analysis.

$$CAPEX_{updated} = CAPEX + C_{additional} \tag{B.10}$$

Specific to AP AEC, we calculate the CAPEX based on established heuristics by the literature and the electricity demand required to electrolyze water.

$$C_{additional_{AP\ AEC}} = \left[\frac{M_{H_2} \times h_{H_2}^{LHV} \times 1000}{\eta_{AEC}}\right] * C_{AEC} \tag{B.11}$$

Table B-2: Values for x_z excluding WC_j.

Input Name	Value	Unit	Source
$C_{I\&C}$	uniform(0.08, 0.55)	% Purchased equipment (PE)	(Peters et al., 2003)
C_p	uniform(0.1, 0.8)	% PE	

[2] See SI D and E for calculations related to the wind farm and battery storage system.

C_{el}	uniform(0.1, 0.4)	% PE	
C_b	uniform(0.1, 0.7)	% PE	
$C_{sf\&yi}$	uniform(0.05, 0.18)	% PE	
C_{land}	900000	$	(Lewis et al., 2022)
C_{eng}	uniform(0.05, 0.3)	% PE	
C_L	uniform(0.03, 0.05)	% PE	
C_c	uniform(0.3, 0.4)	% PE	(Peters et al., 2003)
C_{co}	uniform(0.35, 0.45)	% PE	
C_{WC}	uniform(0.1, 0.2)	% FCI	
C_{AEC}	2026: uniform (750, 1000) 2033: uniform (500, 1000)	$/kWe	(Böhm et al., 2020; IRENA, 2020; Schmidt et al., 2017)

Table B-3: EC_{u_j} and EC_{i_j} for each technology.

Input Name	Value[A]	Unit	Source
AP SMR	(726947344.6, 508096133.6)	$	Calculated
AP CCS	(1103130442, 781847023.7)	$	Calculated
AP BH2S	(940144529.3, 5080528806470)	$	Calculated
AP AEC	(567914373, 402707562.8)	$	Calculated

[A] The first value in the parenthesis is EC_{i_j} and the second is EC_{u_j}. Obtained from Excel file called ***AP_NE_Equipment_List.xlsx***.

B.3. Model Formulation OPEX

The OPEX is partitioned into two parts. A market-dependent OPEX($MDOPEX_j$) and a market-independent (MI) OPEX($MIOPEX_j$). These two values are combined to derive the $OPEX_j$ for each technology option considered.

The $\boldsymbol{OPEX_j}$ is generally divided into fixed and variable costs. The fixed costs represent costs related to labor, overhead, maintenance, and insurance while the variable costs rely on the raw materials and utility costs. In the methodology we utilize, the fixed and variable costs are added together. From this combined quantity, we add another set of cost factors.

Some raw materials and utilities have costs that vary with the market; hence the variable costs are split between the $\boldsymbol{MDOPEX_j}$ and $\boldsymbol{MIOPEX_j}$. All the fixed costs are within the $\boldsymbol{MIOPEX_j}$.

$$\boldsymbol{OPEX = MIOPEX + MDOPEX} \quad \text{(B.12)}$$

B.1.1. Model Formulation OPEX

Table B-4: Nomenclature for the OPEX section.

Parameters	Description	Units
$\boldsymbol{MDOPEX_j}$	Market dependent OPEX for technology $\boldsymbol{j}$	\$/month
$\boldsymbol{MIOPEX_j}$	Market independent OPEX for technology $\boldsymbol{j}$	\$/month
$\boldsymbol{H_{shift}}$	Hours per shift	Hour/shift
$\boldsymbol{H_{dp}}$	Hours per day per processing step	Hours/day/processing step
$\boldsymbol{P_s}$	Processing steps	Processing step
$\boldsymbol{F_a}$	Availability factor	%
$\boldsymbol{wage_h}$	Operator salary	\$/hr
$\boldsymbol{L_c}$	Monthly operator labor cost	\$/month
$\boldsymbol{TL_{c_j}}$	Total labor costs	\$/month
$\boldsymbol{TF_{c_j}}$	Fixed charges	\$/month
$\boldsymbol{FC_j}$	Fixed cost	\$/month
$\boldsymbol{C_{sup}}$	Supervision costs to calculate total labor costs	$\%\boldsymbol{L_c}$

C_{os}	Operating supply costs to calculate total labor costs	% $FCI_j \times \frac{C_{MT}}{12}$
C_{LC}	Laboratory charges to calculate total labor costs	%L_c
$C_{P\&R}$	Patient and royalty costs to calculate total labor costs	% $CAPEX_j$
C_{OH}	Overhead costs to calculate total labor costs	% maintenance + supervision + labor
C_{fin}	Financing fixed cost	% $CAPEX_j$
C_{rent}	Rent fixed cost	%C_{land}
C_{ptax}	Local property tax fixed cost	% TL_c
C_{admin}	Administrative fixed cost	%C_{admin}
C_{ins}	Insurance costs	% FCI_j
C_{MT}	Maintenance costs to calculate total labor costs	%FCI_j
VC_j	Variable cost	$/month
S_{H_2O}	Water cost	$/kg
M_{H_2O}	Process water demand per month	Kg/month
$Misc_j$	Miscellaneous costs in calculating OPEX	$/month
$M_{H_2O_{osmosis}}$	Feedstock water demand	$/kg
$S_{H_2O_{osmosis}}$	Reverse Osmosis water cost	Kg/month
i	Commodity index	
$P_i(T)$	GBM price function for commodity i	$/unit i

$\boldsymbol{P(T=0)_i}$	Initial price of commodity $\boldsymbol{i}$	\$/unit $\boldsymbol{i}$
$\boldsymbol{\mu_i}$	Drift for commodity $\boldsymbol{i}$	%
$\boldsymbol{\sigma_i}$	Volatility for commodity $\boldsymbol{i}$	%
$\boldsymbol{F_{DM}}$	Distribution and marketing costs	\$
$\boldsymbol{F_{RD}}$	R&D costs	\$
$\boldsymbol{M_{NG}}$	Energy flowrate of natural gas	mmBTU/year
$\boldsymbol{M_{EL}}$	Electricity demand	kWh/year
$\boldsymbol{OPEX_j}$	Operational Expenditure for technology $\boldsymbol{j}$	\$

B.3.1. Market Independent OPEX

B.3.1.1. Fixed Costs

The monthly cost of labor was calculated assuming a number of hours per day per processing step, $\boldsymbol{H_{dp}}$. Then dividing by the hours per shift, $\boldsymbol{H_{shift}}$, multiplying by the number of processing steps, $\boldsymbol{P_s}$, times 7 days in a week over 5 shifts per week per operator, gives the number of operators assuming each operator can cover one shift per day. This is the first factor in the square brackets. The resulting hours an operator will work (5 shifts, 8 hours each) results in 40 hours per week. The hourly wage, $\boldsymbol{wage_h}$, times 40 results in the weekly cost of an operator. This is the second factor in the square brackets. Finally, the weekly cost of labor (number of operators times the weekly cost per operator) is converted to the monthly cost of labor through the factor, $\frac{52}{12} * \boldsymbol{F_a}$; where $\boldsymbol{F_a}$ is the availability factor.

$$\boldsymbol{L_c} = \left[\left(\frac{\boldsymbol{H_{dp}}}{\boldsymbol{H_{shift}}}\right) \times \boldsymbol{P_s} \times \frac{\boldsymbol{7}}{\boldsymbol{5}}\right] \times [\boldsymbol{40} \times \boldsymbol{wage_h}] \times \frac{\boldsymbol{52}}{\boldsymbol{12}} \times \boldsymbol{F_a} \tag{B.13}$$

The total labors costs are a function of the $\boldsymbol{L_c}$, $\boldsymbol{CAPEX_j}$, cost factors. Hence, we introduce the total labor costs, $\boldsymbol{TL_c}$:

$$\begin{aligned}\boldsymbol{TL_{c_j}} = \boldsymbol{L_c}\left(\boldsymbol{1} + \boldsymbol{C_{sup}} + \boldsymbol{C_{LC}}\right) + \boldsymbol{FCI_j} \times \frac{\boldsymbol{C_{MT}}}{\boldsymbol{12}} + \left(\boldsymbol{FCI_j} \times \frac{\boldsymbol{C_{MT}}}{\boldsymbol{12}}\right) \times \boldsymbol{C_{OS}} \\ + \boldsymbol{CAPEX_j} \times \frac{\boldsymbol{C_{P\&R}}}{\boldsymbol{12}} + \left(\boldsymbol{L_c}\left(\boldsymbol{1} + \boldsymbol{C_{sup}}\right) + \boldsymbol{FCI_j} \times \frac{\boldsymbol{C_{MT}}}{\boldsymbol{12}}\right) \times \boldsymbol{C_{OH}}\end{aligned} \tag{B.14}$$

There are also fixed charges, $\boldsymbol{TF_c}$:

$$TF_{c_j} = \frac{C_{fin}}{12} \times CAPEX_j + \frac{C_{rent}}{12} \times C_{land} + \frac{C_{ins}}{12} \times FCI_j + \frac{C_{ptax}}{12} \times FCI_j + C_{admin} \times TL_c \quad \text{(B.15)}$$

After obtaining TL_{c_j} and TF_{c_j}, we can calculate the fixed cost, FC:

$$FC_j = TL_{c_j} + TF_{c_j} \quad \text{(B.16)}$$

B.3.1.2. Variable Costs (market independent)

The utility costs portion of the $MI\ OPEX_j$ is only the water costs since electricity is a market-dependent parameter. For SMR, CCS, and BH2S, equation (B.17) applies. We also add miscellaneous costs, which account for other raw materials (catalysts, column trays, solvents, water treatment, etc.). These miscellaneous costs are found in the original reports (see SI A). We define the variable costs, VC_j, as:

$$VC_j = S_{H_2O} \times M_{H_2O_j} + Misc_j \quad \text{(B.17)}$$

If the process is AP AEC, the water dedicated to feedstock is water by reverse osmosis and is more expensive. Hence, for AP AEC, the following equation applies.

$$VC_{j=AP\ AEC} = S_{H_2O} \times M_{H_2O_j} + S_{H_2O_{osmosis}} \times M_{H_2O_{osmosis_j}} + Misc_j \quad \text{(B.18)}$$

B.3.1.3. MIOPEX

With the previous definitions, the $MI\ OPEX_j$ is defined as:

$$MI\ OPEX_j = FC_j + VC_j \quad \text{(B.19)}$$

B.3.2. Market Dependent OPEX

The objective is to use geometric Brownian motion (GBM) to model natural gas, electricity, and ammonia prices with parameters including the drift, μ_i, and volatility, σ_i, for commodity i. We used a bivariate distribution for ammonia and natural gas prices so that we could set a correlation parameter between the two commodities. The correlation was calculated using industrial natural gas prices and ammonia price indices from December 2014 to January 2023 (Bureau of Labor Statistics, 2023; EIA, 2023b).

$$P_i(T) = P(T = 0)_i \prod_{T=0}^{L} [N(1 + \mu_i, \sigma_i)] \quad \text{(B.20)}$$

Distribution and marketing costs (F_{DM}) and R&D (F_{RD}) costs are dependent on the variable costs. The $MDOPEX_j$ can be defined as:

$$\boldsymbol{MDOPEX_j(T) = M_{NG} * P_{NG}(T) + M_{EL} * P_{EL}(T) + MIOPEX_j + (F_{DM} + F_{DM} * F_{RD})} \\ \boldsymbol{\left(M_{NG} * P_{NG}(T) + M_{EL} * P_{EL}(T) + MIOPEX_j\right)} \quad \text{(B.21)}$$

where $\boldsymbol{M_{NG}}$ is the energy flowrate of natural gas in mmBTU/year, and $\boldsymbol{M_{EL}}$ is the electricity demand in kWh/year. The term, $\boldsymbol{M_{NG} * P_{NG}(T) + M_{EL} * P_{EL}(T) + MIOPEX_z}$, is the manufacturing cost. If it is the year when operations start, then start-up costs are added to the $\boldsymbol{MDOPEX_j(T)}$ (see Table B-8). More details on $\boldsymbol{T}$ and financial analysis in Section C.

B.3.3. Inputs for OPEX

Table B-5: Number of processing steps by technology.

Input Name	Value	Unit	Source
AP SMR	30	-	-
AP CCS	33	-	-
AP BH2S	38	-	-
AP AEC	23	-	-
H_{dp}	55		

Processing steps of each AP process. Used for labor cost calculations. All values are assumptions estimated from the process flow diagrams of Lewis et al. (2022), Spath et al. (2005), Brasington et al. (2011), and Young et al. (2021).

Table B-6: Heuristics factors for OPEX.

Input Name	Value	Unit	Source
$\boldsymbol{C_{MT}}$	0.0286	% $\boldsymbol{CAPEX_j}$	(Peters et al., 2003)
$\boldsymbol{C_{sup}}$	0.15	%$\boldsymbol{L_c}$	
$\boldsymbol{C_{os}}$	0.1	% $\boldsymbol{FCI_j \times \frac{C_{MT}}{12}}$	
$\boldsymbol{C_{LC}}$	0.15	% $\boldsymbol{L_c}$	
$\boldsymbol{C_{P\&R}}$	0.005	% $\boldsymbol{CAPEX_j}$	
$\boldsymbol{C_{OH}}$	0.70	%maintenance + supervision + labor	
$\boldsymbol{C_{fin}}$	0	% $\boldsymbol{CAPEX_j}$	
$\boldsymbol{C_{rent}}$	0.1	%$\boldsymbol{C_{land}}$	
$\boldsymbol{C_{ptax}}$	0.005	% $\boldsymbol{FCI_j}$	
$\boldsymbol{C_{admin}}$	0.025	% $\boldsymbol{TL_c}$	

C_{ins}	0.2	% FCI_j	

Table B-7: Miscellaneous raw materials costs.

Input Name	Value	Unit	Source
AP SMR	6824075.7	$/year	(Brasington et al., 2011; Lewis et al., 2022; A. F. Young et al., 2021)
AP CCS	12434783.5	$/year	
AP BH2S	27093089.5	$/year	
AP AEC	335267.1	$/year	

Table B-8: Start-up costs

Input Name	Value	Unit	Source
AP SMR	15413897.7	$	(Brasington et al., 2011; Lewis et al., 2022)
AP CCS	16514194.1	$	
AP BH2S	15532525.5	$	
AP AEC	118627.7	$	

Table B-9: GBM inputs.

Input Name	Value	Unit	Source
$P_{NG}(T=0)$	7.753	$/mmBTU	(EIA, 2023a)
$\mu_{NG}{}^{A}$	-0.0016	-	
σ_{NG}	0.039683	-	
$P_{EL}(T=0)$	0.083	$/kWh	
$\mu_{EL}{}^{A}$	-0.0006	-	
σ_{EL}	0.00536	-	

[A] The drift terms were obtained by calibrating the GBM model to the average price of commodity i in 2050 to the EIA's Annual Energy Outlook 2023 predictions (EIA, 2023a). Electricity was picked as the industrial electricity price in the baseline scenario. Natural gas was picked as the industrial natural gas price in the baseline scenario.

C. Stochastic DCF Model Based on Techno-Economic Quantities

C.1. Problem statement

This analysis employs a Stochastic Discounted Cash Flow (DCF) model to evaluate the economic viability of various technology pathways for ammonia production. This assessment aims to provide a comprehensive understanding of the economic performance by considering various uncertain factors and their impact on the Net Present Value ($\boldsymbol{NPV}$) per lifetime ammonia produced metric. The NPV calculation factors in different cash flows, discount rates, and probabilities, enabling a robust evaluation of the pathways in a stochastic context.

The nomenclature for a Stochastic Discounted Cash Flow (DCF) model encompasses key financial and economic parameters used to evaluate investments and projects under uncertain conditions. These parameters define discount rates, costs, revenues, emissions, and various financial factors. These parameters are essential for assessing the potential financial outcomes of an investment while considering factors like inflation, tax credits, cash flows, and environmental impacts.

Table C-1: Nomenclature for DCF section.

Parameters	*Description*	*Units*
$\boldsymbol{d_p}$	Private discount rate	%
$\boldsymbol{d_s}$	Social discount rate	
$\boldsymbol{e}$	equity	-
$\boldsymbol{R_e}$	cost of equity	-
$\boldsymbol{R_d}$	cost of debt	-
$\boldsymbol{\varphi_{state}}$	state income taxes	$
$\boldsymbol{\varphi_{federal}}$	federal income taxes	$
$\boldsymbol{r}$	interest rate	%
$\boldsymbol{M_{NH3}}$	Monthly ammonia production	Tonne/day

$\boldsymbol{S}$	Month of project start	month
$\boldsymbol{C}$	Construction time	months
$\boldsymbol{L}$	Operating lifetime (duration)	months
$\boldsymbol{NPV}$	Net Present Value	$
$\boldsymbol{CF(T)}$	cash flow at time T	$
$\boldsymbol{Land(T)}$	costs of purchasing land at time T	$
$\boldsymbol{C_{land}}$	Land cost	$
$\boldsymbol{WC(T)}$	costs of injecting working capital at time T	$
$\boldsymbol{L_{loan}}$	loan lifetime	years
$\boldsymbol{H_y}$	Hours per year (365 * 24)	hour/year
$\boldsymbol{CI_{j_{direct}}}$	direct emission	kgCO2/KgH2
$\boldsymbol{CI_{j_{NG}}}$	Natural gas emission	kgCO2/KgH2
$\boldsymbol{CI_{j_{Biomass}}}$	Biomass emission	kgCO2/KgH2
$\boldsymbol{X_{oil}(T)}$	electric demand from oil over the hydrogen production	kgCO2/kWh_e
$\boldsymbol{X_{nuclear}(T)}$	electric demand from nuclear over the hydrogen production	kgCO2/kWh_e
$\boldsymbol{X_{renewables}(T)}$	electric demand from renewables over the hydrogen production	kgCO2/kWh_e
$\boldsymbol{X_{NG}(T)}$	electric demand from NG over the hydrogen production	kgCO2/kWh_e

$\boldsymbol{X_{coal}(T)}$	electric demand from coal over the hydrogen production	kgCO2/kWh_e
$\boldsymbol{Sales(T)}$	revenue stream from selling ammonia at time T	$
$\boldsymbol{Credits_{CE}(T)}$	cash-equivalent tax credits	-
$\boldsymbol{F_{45V}(CI_j)}$	intensive tax credits per unit of H_2 captured	-
$\boldsymbol{F_{45Q}}$	intensive tax credits per unit of CO_2 captured	-
$\boldsymbol{L_{equipment}}$	equipment lifetime	years
$\boldsymbol{C_{uninstalled\ equipment}}$	costs of uninstalled equipment	$
$\boldsymbol{\eta_{NGCC}}$	NGCC thermal efficiency	%

C.2. DCF Model Formulation

The economic performance of each technology pathway was assessed using a Net Present Value ($\boldsymbol{NPV}$) per lifetime ammonia produced metric. NPV is the sum of the present value of all cash flows at each period (monthly basis) over the lifetime amount of ammonia production, $\boldsymbol{M_{NH3}}$.

$$\boldsymbol{NPV} = \frac{\mathbf{1}}{\boldsymbol{M_{NH3}}} \sum_{\boldsymbol{T=S}}^{\boldsymbol{S+C+L}} \frac{\boldsymbol{CF(T)}}{(\mathbf{1}+\frac{\boldsymbol{d_p}}{\mathbf{12}})^{\boldsymbol{T-S}}} \quad \text{(C.1)}$$

where $\boldsymbol{CF(T)}$ is the cash flow at time $\boldsymbol{T}$. The public discount rate, d_p, was calculated as the weighted average cost of capital (WACC) (C.2); as shown below; $\boldsymbol{e}$ is the equity, $\boldsymbol{R_e}$ is the cost of equity, $\boldsymbol{R_d}$ is the cost of debt, and $\boldsymbol{\varphi_{state}} + \boldsymbol{\varphi_{federal}}$ are the state and federal income taxes, respectively.

$$\boldsymbol{d_p} = \boldsymbol{e} * \boldsymbol{R_e} + ([\mathbf{1}-\boldsymbol{e}] * \boldsymbol{R_d} * [\mathbf{1} - (\boldsymbol{\varphi_{state}} + \boldsymbol{\varphi_{federal}})]) \quad \text{(C.2)}$$

$$\boldsymbol{CF(T) = FCI(T)}^{3} \boldsymbol{+ Land(T) + WC(T) + PMT(T)} \\ \boldsymbol{+ Sales(T) + OPEX(T) + Tax(T) + Credits_{CE}(T)} \quad \text{(C.3)}$$

Equations (C.4)-(C.6) represent the staggered spending of the FCI to build the ammonia plant over three years ($\boldsymbol{C}$ months). $\boldsymbol{Y_1}$,$\boldsymbol{Y_2}$,and $\boldsymbol{Y_3}$are the fraction of the FCI that is spent on a given year.

$$\boldsymbol{FCI}\left(\boldsymbol{0 < T \leq \frac{C}{3}}\right) = \boldsymbol{-Y_1 * \frac{FCI_j}{12}} \quad \text{(C.4)}$$

$$\boldsymbol{FCI}\left(\boldsymbol{\frac{C}{3} < T \leq \frac{2C}{3}}\right) = \boldsymbol{-Y_2 * \frac{FCI_j}{12}} \quad \text{(C.5)}$$

$$\boldsymbol{FCI}\left(\boldsymbol{\frac{2C}{3} < T \leq C}\right) = \boldsymbol{-Y_3 * \frac{FCI_j}{12}} \quad \text{(C.6)}$$

$\boldsymbol{Land(T)}$ and $\boldsymbol{WC(T)}$ are the costs of purchasing land and injecting working capital to begin operation.

$$\boldsymbol{Land(T = S) = -C_{land}}\,, \boldsymbol{Land(T = S + C + L) = C_{land}} \quad \text{(C.7)}$$

$$\boldsymbol{WC(T = S + C) = -WC_J},\ \boldsymbol{WC(T = S + C + L) = WC_j} \quad \text{(C.8)}$$

Equations (C.9)-(C.11) represent increasing interest payments as the amount of borrowed capital increases throughout the construction period and (C.12) the constant payments to pay off the loan.

$$\boldsymbol{PMT}\left(\boldsymbol{S < T \leq S + \frac{C}{3}}\right) = \boldsymbol{-\left(\frac{r}{12}\right) * T * (1 - e) * Y_1 * \frac{FCI_j}{12}} \quad \text{(C.9)}$$

$$\boldsymbol{PMT}\left(\boldsymbol{S + \frac{C}{3} < T \leq S + \frac{2C}{3}}\right) = \boldsymbol{-\left(\frac{r}{12}\right) * (1 - e) * [(T - (S + \frac{C}{3})) * Y_2 * \frac{FCI_j}{12} + Y1 * FCI_j]} \quad \text{(C.10)}$$

$$\boldsymbol{PMT}\left(\boldsymbol{S + \frac{2C}{3} < T \leq S + C}\right) = \boldsymbol{-\left(\frac{r}{12}\right) * (1 - e) * [(T - (\frac{2C}{3} + S)) * Y_3 * \frac{FCI_j}{12} + (Y_1 + Y_2) * FCI_j]} \quad \text{(C.11)}$$

[3] If the start of the plant is the year 2030, then the equity part of the FCI appreciates at the risk-free rate (4.25%) for seven years. The appreciation is compounded monthly. The ROI after seven years of appreciation is subject to income tax (set as 21%).

$$\boldsymbol{PMT(S+C<T\leq S+C+L_{loan})=-FCI_j\times\frac{r}{1-(1-r)^{12*L_{loan}}}} \quad \text{(C.12)}$$

$\boldsymbol{Sales(T)}$ and $\boldsymbol{OPEX(T)}$ represent the revenue stream from selling ammonia to the market and the cost of operating the plant respectively.

$$\boldsymbol{Sales(S+C<T\leq S+C+L)=M_{NH3}\cdot*\frac{F_A*\frac{H_y}{24}}{12}*P_{NH_3}(T)} \quad \text{(C.13)}$$

$$\boldsymbol{OPEX(S+C<T\ \leq S+C+L)=OPEX_j(T)} \quad \text{(C.14)}$$

where $\boldsymbol{L_{loan}}$ is the loan lifetime in years, $\boldsymbol{F_a*H_y}$ are the operating hours per year, $\boldsymbol{M_{NH3}}\cdot$ is the monthly ammonia production and $\boldsymbol{C_{NH3}(T)}$ its market-dependent cost.

$\boldsymbol{Tax(T)}$ is the income tax and $\boldsymbol{Credits_{CE}(T)}$ represents the cash-equivalent IRA tax credits. The following variables are interconnected in the financial analysis of income and expenses, with depreciation and uninstalled equipment cost playing key roles in determining net revenue and, subsequently, tax.

$$\boldsymbol{Tax\ (S+C<T<S+C+L)=-(Net\ revenue(T))*(\varphi_{state}+\varphi_{federal})} \quad \text{(C.15)}$$

$$\begin{aligned}\boldsymbol{Net\ revenue(S+C\leq T\leq S+C+L)}&\\ \boldsymbol{=Depreciation\left(S+C\leq T\leq S+C+L_{equipment}\right)}&\\ \boldsymbol{+OPEX(T)+Sales(T)+PMT(T)}&\end{aligned} \quad \text{(C.16)}$$

$$\boldsymbol{Depreciation(T)=\left(\frac{100\%}{L_{equipment}}\right)*EC_{u_j}} \quad \text{(C.17)}$$

C.3. Policy Model

C.3.1. Carbon Intensity Calculations

The calculation of the carbon intensity as a function of time, $\boldsymbol{CI_j(T)}$, the carbon intensity is divided into multiple components. Each component is in units $\frac{\boldsymbol{Kg_{CO_2}}}{\boldsymbol{Kg_{H_2}}}$ in (C.18). The electric grid carbon intensity (C.19) in $\frac{\boldsymbol{Kg_{CO_2}}}{\boldsymbol{Kg_{H_2}}}$ is the electric mix weighted average of the carbon intensities of each type of electric generation times the electric demand of the technology $\boldsymbol{j}$ over the hydrogen production. In this study, we use the electricity demand of hydrogen only because the tax credits only depend on the emissions of hydrogen.

$$CI_j(T) = CI_{j_{direct}} + CI_{j_{NG}} + CI_{j_{Biomass}} + CI_{j_{Electricity}}(T) \quad \text{(C.18)}$$

$$CI_{j_{Electricity}}(T) = \left[X_{oil}(T) * CI_{elec_{oil}} + X_{nuclear}(T) * CI_{elec_{nuclear}} + X_{renewables}(T) * CI_{elec_{nuclear}} + X_{NG}(T) * CI_{elec_{NG}} + X_{coal}(T) * CI_{elec_{coal}}\right] \quad \text{(C.19)}$$

The natural gas carbon intensity of SMR and CCS are estimated from the upstream emissions per kWh of electricity of an NGCC plant times the average efficiency of an NGCC plant (see Table C-3). The direct, or stack, emissions, $CI_{j_{direct}}$, from SMR and CCS come from Lewis et al. (2022) and are assumed to be 0 for BH2S and AEC.

$$CI_{SMR_{NG}} = CI_{elec_{NG}} \times \eta_{NGCC} \times \frac{\frac{\dot{M}_{NG_j}}{365}}{M_{H_2} \times h_{NG}^{LHV} \times \left[0.000948 \frac{MMBtu}{MJ}\right] \times \left[1000 \frac{kg}{tonne}\right]} \quad \text{(C.20)}$$

$$CI_{CCS_{NG}} = CI_{SMR_{NG}} * (1 - R_{CO_2}) \quad \text{(C.21)}$$

$$CI_{j_{Biomass}} = \frac{\dot{M}_{biomass}}{M_{H_2}} * CI_{Biomass} \quad \text{(C.22)}$$

C.3.2. Policy Tax Credits

The AP plan first must decide on a credit program (45V or 45Q). AP BH2S and AP AEC do not qualify for 45Q. Hence, only AP CCS can choose between 45V and 45Q by using the formula below:

$$\max\left[\begin{matrix} 45V: \sum_{T=S+C}^{L+S+C} \mathcal{H}_{CE}\left[\frac{\mathbf{F_{45Q}} * \dot{M}_{H2}\left(CI_{SMR_{direct}} - CI_{j_{direct}}\right)}{(1+d_p)^{T-S}}\right], \\ 45Q: \sum_{T=S+C}^{L+S+C} \mathcal{H}_{CE}\left[\frac{\dot{M}_{H2} * F_{45V}(CI_j)}{(1+d_p)^{T-S}}\right] \end{matrix}\right] \quad \text{(C.23)}$$

where $\mathcal{H}_{CE}$ is an operator that converts the tax credits from the IRA eligible tax credits to the cash-equivalent utilizing the "direct pay" and "transferability" capabilities of the credits – it performs the logical operation in equations (C.26) and (C.27). The first term in the max function is the NPV of 45V credits. The second term is the NPV of 45Q credits.

$$\boldsymbol{Credits_{45V_j}(T) = \dot{M}_{H2} * F_{45V}(CI_j)} \quad \text{(C.24)}$$

$$\boldsymbol{Credits_{45Q_j}(T) = \mathbf{F_{45Q}} * \dot{M}_{H2}\left(CI_{SMR_{direct}} - CI_{j_{direct}}\right)} \quad \text{(C.25)}$$

$$\boldsymbol{Credits_{CE}\ (T|\ |Tax(T)| > Credits(T)\ ) = Credits_j(T)} \quad \text{(C.26)}$$

$$\boldsymbol{Credits_{CE}\ (T|\ |Tax(T)| < Credits(T)\ ) = -Tax(T)} \quad \text{(C.27)}$$
$$\boldsymbol{+F_t(T) * (Credits_j(T) + Tax(T))}$$

where $\boldsymbol{F_{45V}(CI_j)}$ and $\boldsymbol{F_{45Q}}$ is the intensive tax credits per unit of H_2 produced and CO_2 captured, respectively. 45V is a piecewise function of CI. 45V and 45Q are mutually exclusive, so the highest tax credit is preferred for technology option $\boldsymbol{j}$. $\boldsymbol{\dot{M}_{H2}}$ is the monthly flowrates of H_2 and CO_2. $\boldsymbol{F_t(T)}$ is an exchange rate of USD per tax credit. It is equal to 1 in the first five years of operation (due to direct pay) and then attains a market values of less than one after five years. $\boldsymbol{F_{45V}(CI_j)}$ and $\mathbf{F_{45Q}}$ become zero after 10 and 12 years of operation, respectively.

C.4. Measurement Metric Formulations

Table C-2: Nomenclature

Parameters	Description	Units
$\boldsymbol{CAC_j}$	Carbon abatement cost for technology $\boldsymbol{j}$	$/tCO2eq
$\boldsymbol{d_s}$	Social discount rate	%
$\boldsymbol{TC_{j_\alpha}}$	Tax credit for technology $\boldsymbol{j}$ for type of credit $\boldsymbol{\alpha}$	$/Kg H2
$\boldsymbol{\alpha}$	Can be the potential tax credits discounted at $\boldsymbol{d_s}$, cash-equivalent tax credits discounted at $\boldsymbol{d_s}$, or cash-equivalent tax credits discounted at $\boldsymbol{d_p}$	
$\boldsymbol{L_{H_2}}$	Lifetime of hydrogen produced under the IRA.	months

C.4.1. Carbon Abatement Cost

A valuable measure in the context of comparisons of climate policy instruments could be the carbon abatement cost ($\boldsymbol{CAC_j}$), which quantifies the cost to the taxpayer of bringing low-carbon technologies to commercialization, normalized by the mitigated emissions over the lifetime of the plant (see eq.5).

$$\boldsymbol{CAC_j = \sum_{T=S+C}^{L+S+C} \frac{\frac{Credits_{j(T)}}{[1+d_s]^{T-S}}}{\sum_{T=S+C}^{L+S+C}\left[\frac{M_{\cdot H2}\left(CI_{SMR}(T) - CI_j(T)\right)}{[1+d_s]^{T-S}}\right]}} \quad \text{(C.28)}$$

where $\boldsymbol{L+S+C}$ represents the operating lifetime, the month the plant begins to be built, and the construction period, respectively. The denominator represents the total abated emissions as a Riemann sum of the CO_2 at all periods. Both the carbon and credits are discounted to the present value at the social discount rate, $\boldsymbol{d_s}$. The discount rate for the CAC is set to two percent – in line with EPA's estimates of the social cost of carbon (EPA, 2022).

C.4.2. Tax Credits on a Hydrogen Basis

Much like the $\boldsymbol{CAC_j}$, the total tax credits we measure are on a hydrogen basis. This metric is easily compared to the popular levelized cost of hydrogen (LCOH) metric. We develop the following metrics to quantify the three types of tax credit ($\boldsymbol{TC_{j_\alpha}}$) quantifications we report:

$$\boldsymbol{TC_{j_{Potential\ (2\%)}} = \sum_{T=S+C}^{L+S+C} \frac{\frac{Credits_{j(T)}}{\left[1+\frac{d_s}{12}\right]^{T-S}}}{\sum_{T=S+C}^{S+C+L_{H_2}}\left[\frac{M_{\cdot H2}}{\left[1+\frac{d_s}{12}\right]^{T-S}}\right]}} \quad \text{(C.29)}$$

$$\boldsymbol{TC_{j_{CE\ (2\%)}} = \sum_{T=S+C}^{L+S+C} \frac{\frac{Credits_{CE_{j(T)}}}{\left[1+\frac{d_s}{12}\right]^{T-S}}}{\sum_{T=S+C}^{S+C+L_{H_2}}\left[\frac{M_{\cdot H2}}{\left[1+\frac{d_s}{12}\right]^{T-S}}\right]}} \quad \text{(C.30)}$$

$$\boldsymbol{TC_{j_{CE\ (9.3\%)}} = \sum_{T=S+C}^{L+S+C} \frac{\frac{Credits_{CE_{j(T)}}}{\left[1+\frac{d_p}{12}\right]^{T-S}}}{\sum_{T=S+C}^{S+C+L_{H_2}}\left[\frac{M_{\cdot H2}}{\left[1+\frac{d_p}{12}\right]^{T-S}}\right]}} \quad \text{(C.31)}$$

We take the NPV of the tax credits from the public and private perspective. $TC_{j_{Potential\ (2\%)}}$ captures the total amount of credits issued – hence the cost to the taxpayer. $TC_{j_{CE\ (2\%)}}$ is always less than $TC_{j_{Potential\ (2\%)}}$ and represent the amount of tax credits awarded to the low-carbon AP investor from the total pool of tax credits, $TC_{j_{Potential\ (2\%)}}$. $TC_{j_{CE\ (9.3\%)}}$ is the low-carbon AP investor's valuation of the tax credits using the WACC as the discount rate. The AP investor is more "impatient" than the government and hence places more value on credits awarded in the near future.

C.5. Data sources

Table C-3: Direct carbon emissions intensity

Input Name	Value	Unit	Source
$CI_{SMR_{direct}}$	9.3	Kg CO2/Kg H2	(Lewis et al., 2022)
η_{NGCC}	46.1%[a]	-	(O'Donoughue et al., 2014)[b]

[a] The thermal efficiency was used to back-calculate the upstream emissions from natural gas from NGCC plants. An NGCC plant demands an amount of natural gas that is equal to the amount of energy input needed to generate electricity. Since we have the carbon intensity of NGCC generation, we can derive the natural gas upstream emissions by dividing by thermal efficiency.

[b] The thermal efficiency is the average efficiency of NGCC plants in the US from Table 1 of O'Donoughe et al. (2013).

Table C-4: Carbon intensity inputs for electricity mix.

Input Name	Value	Unit	Source
$X_{oil}(T)$	uniform(0.256, 1.17)	Kg CO2/Kg H2	(Nicholson & Heath, 2021)
$X_{NG}(T)$	uniform(0.389, 0.988)	Kg CO2/Kg H2	
$X_{Coal}(T)$	uniform(1.001,1.01)	Kg CO2/Kg H2	
$X_{nuclear}(T)$	uniform(0.012, 0.220)	Kg CO2/Kg H2	
$X_{renewables}(T)$	0	Kg CO2/Kg H2	

Table C-5: Financial inputs

Input Name	Value	Unit	Source
F_a	0.9	-	(Lewis et al., 2022)
Y_1, Y_2, Y_3	10%, 60%, 30%	-	Author's assumption

R_e	12.27%	-	
R_d	5.5%	-	(Damodaran, 2023)
e	63.19%	-	
φ_{state}	5.25%	-	
$\varphi_{federal}$	21%	-	
L_{loan}	180	years	(Lewis et al., 2022)
$L_{equipment}$	84	years	(Turton et al., 2018)

Table C-6: IRA Inputs

Input Name	Value	Unit	Source
$F_{45V}(0 - 0.45 \frac{\mathbf{KgCO_{2_{eq}}}}{\mathbf{Kg_{H2}}})$	3	$/Kg H2	IRA , 2022
$F_{45V}0.45 - 1.5 \frac{\mathbf{KgCO_{2_{eq}}}}{\mathbf{Kg_{H2}}})$	1	$/Kg H2	IRA, 2022
$F_{45V}(1.5 - 2.5 \frac{\mathbf{KgCO_{2_{eq}}}}{\mathbf{Kg_{H2}}})$	0.75	$/Kg H2	IRA, 2022
$F_{45V}(2.5 - 4.0 \frac{\mathbf{KgCO_{2_{eq}}}}{\mathbf{Kg_{H2}}})$	0.6	$/Kg H2	IRA, 2022
F_{45Q}	85	$/tCO2e	IRA, 2022

Table C-7: Measurement metrics values.

Input Name	Value	Unit	Source
d_s	2%	%/year	(EPA, 2022)
L_{H_2}	120[A]	months	IRA, 2022

[A] The lifetime of 45V credits (10 years) is assumed to be the lifetime of hydrogen production under the IRA.

D. Wind Farm and Battery System Optimization

D.1. Problem Statement

The problem aims to minimize the capital cost required for wind and battery installations to meet constant electricity demand. Optimal sizing of wind and battery capacity depends on the relative costs of wind and battery facilities, wind generation resource availability, and requirements for constant electricity output. Thus, the objective is to find the optimal capacities of wind and battery installations that minimize the overall capital cost.

D.2. Model Formulation

In this problem, the index $\boldsymbol{t} \in \boldsymbol{N}$ denotes discrete time steps. We model hourly (i.e., 8760 time steps) and monthly (i.e., 12 time steps) resolutions. Table D-1 outlines notations used in the formulation, while Table D-2, Table D-3, Table D-4, and Table D-5 summarize numerical input values and their sources.

Table D-1: Nomenclature

	Description	*Units*
Decision variables		
$\boldsymbol{w}$	Installed wind capacity	MW
$\boldsymbol{b}$	Battery capacity	MW
$\boldsymbol{w(t)}$	Wind generation in each time period	MWh
$\boldsymbol{c(t)}$	Battery charge in each time period	MWh
$\boldsymbol{d(t)}$	Battery discharge in each time period	MWh
$\boldsymbol{b(t)}$	Battery state of charge in each time period	MWh
Parameters		
$\boldsymbol{CF(t)}$	Capacity factor of wind across different periods.	Unitless
$\boldsymbol{D}$	Constant electricity demand, which differs based on specific technologies, including AP CCS, AP BH2S, and AP AEC	MWh
$\boldsymbol{EFF}$	Roundtrip efficiency of the battery system. It is assumed to be 85%[A].	Unitless
$\boldsymbol{COST_{wind}}$	Capital cost per MW of wind capacity	$/MW
$\boldsymbol{COST_{battery}}$	Capital cost per MW of battery capacity	$/MW

[A] Cole & Frazier (2019)

D.2.1. Objective Function

The objective function (eq. D.1) is to minimize the total capital investments, which is the sum of the capital cost of wind installation ($\boldsymbol{COST_{wind}} \times \boldsymbol{w}$) and the capital cost of battery installation ($\boldsymbol{COST_{battery}} \times \boldsymbol{b}$).

$$\min_{\boldsymbol{w \geq 0, b \geq 0}} \boldsymbol{F} = \boldsymbol{COST_{wind}} \times \boldsymbol{w} + \boldsymbol{COST_{battery}} \times \boldsymbol{b} \quad \text{(D.1)}$$

D.2.2. Constraints

The power balance constraint (D.2) ensures that the net power balance in each time period equals the electricity demand ($\boldsymbol{D}$). It accounts for wind generation ($\boldsymbol{w(t)}$), battery charging ($\boldsymbol{c(t)}$), and battery discharging ($\boldsymbol{d(t)}$). The net power balance is achieved by subtracting the battery charge and adding the battery discharge to the wind generation.

$$\boldsymbol{w(t) - c(t) + d(t) = D}, \qquad \forall \boldsymbol{t} \quad \text{(D.2)}$$

Wind generation constraint (D.3) enforces wind generation ($\boldsymbol{w(t)}$) in each time period to not exceed wind resource availability ($\boldsymbol{CF(t) \times w}$).

$$\mathbf{0} \leq \boldsymbol{w}(\boldsymbol{t}) \leq \boldsymbol{CF}(\boldsymbol{t}) \times \boldsymbol{w}, \qquad \forall \boldsymbol{t} \tag{D.3}$$

(D.4) and (D.5) limit the battery charging and discharging to their capacity.

$$\mathbf{0} \leq \boldsymbol{c}(\boldsymbol{t}) \leq \boldsymbol{b}, \qquad \forall \boldsymbol{t} \tag{D.4}$$

$$\mathbf{0} \leq \boldsymbol{d}(\boldsymbol{t}) \leq \boldsymbol{b}, \qquad \forall \boldsymbol{t} \tag{D.5}$$

While (D.6) defines the battery storage state considering roundtrip efficiency, charge and discharge dynamics. Lastly, (D.7) puts a lower and an upper limit on the battery's state of charge.

$$\boldsymbol{b}(\boldsymbol{t}) = \boldsymbol{b}(\boldsymbol{t}-\mathbf{1}) + \boldsymbol{EFF} \times \boldsymbol{C}(\boldsymbol{t}) - \boldsymbol{d}(\boldsymbol{t}), \ \forall \boldsymbol{t} > \mathbf{1} \tag{D.6}$$

$$\mathbf{0} \leq \boldsymbol{b}(\boldsymbol{t}) \leq \boldsymbol{b}, \qquad \forall \boldsymbol{t} \tag{D.7}$$

D.3. Data sources

D.1.1. Sources and assumptions on the capacity factor data.

The data for the wind capacity factors ($\boldsymbol{CF}(\boldsymbol{t})$) is parametrized by location, year, and wind turbine design. The hourly capacity data originates from Pfenninger et al. (2016).

- **Locations**: the capacity factors are obtained from 8 locations, labeled Yara, Koch, Woodward, Port Neal, Verdigris, Nutrien, Donaldson, AdvanSix. The locations match some of the largest AP plants in the US (see Table D-2).
- **Year**: only 2019 data was available. We assume 2019 capacity factors to be a typical meteorological year (TMY) for the AP plant model for computational tractability. In other words, the time-varying results from this optimization problem ($\boldsymbol{w}(\boldsymbol{t})$, $\boldsymbol{d}(\boldsymbol{t})$, etc..) are oscillatory functions in the context of the AP plant (see SI E).
- **Wind turbine design**: as wind turbine technology improves, the costs are expected to decrease and the hub heights and capacity per turbine to increase. 2026 scenario data was obtained using a hub height of 90.2m and a BONUS B82 2300 turbine. 2033 data was obtained using a hub height of 120m and a GAMESA G128 5000 turbine. The turbine design was picked to match closely with the average design specifications of deployed wind turbines in the baseline and moderate scenarios of NREL's Annual Technology Baseline report (Open Energy Data Initiative (OEDI), 2022)[4].

D.1.2. Justification for hybrid wind farm locations and applications to the AP plant model.

Our stochastic NPV model uses a uniform distribution to capture the lower and upper bounds of uncertain variables such as wind and battery capex. To capture the upper and lower bounds of wind resource availability in those eight locations, we compute the average monthly and hourly capacity factors and pick two farm locations each year with the highest and lowest average capacity factors (see Table D-3). Intuitively, locations with low-energy wind resources will have a larger wind capacity (higher overall CAPEX) than locations with high-energy wind resources (lower overall CAPEX).

[4] The average wind turbine specifications reported by NREL were in the years 2020 and 2030. We use the design parameters from 2020 for the 2026 scenario and the 2030 design parameters for our 2033 scenario.

This helps in understanding which locations are performing the best and the worst in wind electricity generation, and these two locations' data are used for stochastic NPV analysis.

Table D-2: Specific locations of AP plants.

Company	*Name*	*State*	*Latitude*	*Longitude*
CF Industries	Donaldsonville Complex	LS	30.087397	-90.955682
CF Industries	Verdigris Complex	OK	36.233335	-95.718833
CF Industries	Woodward Complex	OK	36.437942	-99.472056
CF Industries	Port Neal Complex	IA	42.332879	-96.377213
Koch Industries	Koch Fertilizer Company Enid	OK	36.380941	-97.761921
Nutrien	Nutrien Augusta Nitrogen	GA	33.443125	-81.930376
Yara	BASF Chemicals Division	TX	29.000639	-95.393318
AdvanSix	AdvanSix	VA	37.300405	-77.271941

Table D-3: Capacity factor data for selected locations.

2023				
Location	*Average*	*Minimum*	*Maximum*	*Std Deviation*
Koch	35.5%	0.0%	98.2%	28.1%
AdvanSix	17.8%	0.0%	97.6%	18.9%
Port Neal	34.9%	0.0%	98.2%	27.8%
Nutrien	18.4%	0.0%	98.2%	18.7%
Yara	29.1%	0.0%	98.1%	23.7%
Woodward	39.2%	0.0%	98.2%	29.6%
Donaldson	19.4%	0.0%	98.2%	20.1%
Verdigris	31.4%	0.0%	98.2%	26.7%
2030				
Location	*Average*	*Minimum*	*Maximum*	*Std Deviation*
Koch	42.7%	0.0%	96.4%	29.8%
AdvanSix	26.7%	0.0%	96.4%	23.5%
Port Neal	41.9%	0.0%	96.4%	29.3%
Nutrien	25.4%	0.0%	96.4%	22.5%
Yara	35.7%	0.0%	96.4%	26.0%
Woodward	46.1%	0.0%	96.4%	30.9%
Donaldson	25.8%	0.0%	96.4%	23.2%
Verdigris	38.7%	0.0%	96.4%	28.8%

Constant electricity demand, $\boldsymbol{D}$, is outlined below in Table D-4.

Table D-4: Constant electricity demand of each technology.

	Low	*High*	*Units*	*Low*	*High*	*Units*
AP CCS, $\boldsymbol{D}$	117		MW	922428		MWh/year
AP BH2S, $\boldsymbol{D}$	127		MW	1001268		MWh/year
AP AEC, $\boldsymbol{D}$	1007	913	MW	7939188	7198092	MWh/year

Notes: AP AEC has a demand range because we assume an uncertain electrolyzer efficiency.

The capital cost of wind and battery is based on values from Bistline et al. (2023). See below in Table D-5.

Table D-5: CAPEX of wind and battery systems.

Battery	*Low*	*High*	*Units*
2023, $\boldsymbol{COST}_{battery}$	800	1500	$/kW
2030, $\boldsymbol{COST}_{battery}$	450	1200	$/kW
Wind			
2023, $\boldsymbol{COST}_{wind}$	1200	1400	$/kW
2030, $\boldsymbol{COST}_{wind}$	750	1200	$/kW

D.4. Model implementation

The optimization problem is formulated in Python and solved using the pulp library, a popular open-source linear programming (LP) modeling package that can seamlessly handle mixed-integer linear programming (MILP) scenarios (Dunning et al., 2011).

PuLP offers a simple and intuitive syntax for defining optimization problems using Python, such as intuitive syntax for defining decision variables, objective functions, and constraints. Thus, the model can be formulated to resemble the mathematical notation that describes optimization problems closely. It provides a high-level abstraction that makes it easier to express mathematical programming concepts.

D.5. Results

The optimal results are computed for installed wind capacity, battery capacity, wind generation, battery charging, battery discharging, battery state of charge, storage duration, and wind supply curtailment. These results collectively provide insights into how the optimization model has determined the optimal configuration for wind capacity, battery capacity, and their operational behavior to minimize costs while ensuring supply-demand balance and considering various constraints. We report and publish all results from this optimization in an Excel file – named ***AP_NE_Optimization_Results.xlsx***.

E. Scenario Specific Changes and Assumptions

The previous SI modules describe the model methodology for scenario A in its entirety. This section contains a set of case studies of this model. There are three dimensions to the case studies:

1. Business models: choice between scenarios A, B, and C. Scenario A is the baseline, not discussed in this section.
2. CBAM: a choice on whether to enforce CBAM or not.
3. Electricity matching constraints: a choice to enforce yearly, monthly, or hourly constraints.

This section describes the differences between scenarios B and C from the baseline. We also describe the implementation of CBAM. Finally, we do not discuss matching constraints because the constraints are integrated into the optimization model (see section D)[5].

Table E-1: Nomenclature.

Variables/Parameters	*Description*	*Units*
$\boldsymbol{MIOPEX_{el}(\Gamma)}$	Additional market-independent OPEX as a function of the remainder of the AP plant time attributed to the wind and battery O&M.	\$/month
$\boldsymbol{d_{monthly}(\Gamma)}$	Monthly aggregated sum of the battery discharge	MWh/month
$\boldsymbol{C_{f+v}^{wind}}$	Fixed and variable O&M cost of the wind farm	\$/MW/year
$\boldsymbol{C_{f}^{battery}}$	Fixed O&M costs of the battery system	\$/kW-year
$\boldsymbol{C_{v}^{battery}}$	Variable O&M costs of the battery system	\$/MWh
$\boldsymbol{L}$	Plant operating lifetime	months
$\boldsymbol{S}$	The time step in which the plant construction begins	month
$\boldsymbol{C}$	Construction time	months
$\boldsymbol{S_{el}(T)}$	Surplus electricity income.	\$/month
$\boldsymbol{w_{montly}(\Gamma)}$	Monthly aggregated sum of the total electricity generated by the wind farm.	MWh/month
$\mathbf{LCOE_{wind\ farm\ only}}$,	The levelized cost of electricity of a stand-alone wind farm.	\$/MWh
$\boldsymbol{P_{Electricity}(T)}$	Electricity market price	\$/kWh
$\boldsymbol{48E}$	The percentage ITC of 48E credits from the IRA	%wind and battery CAPEX
$\boldsymbol{45Y(T)}$	Time function of 45Y credits bounded by the start of operations and 45Y credit lifetime, $\boldsymbol{E_{45Y}}$	\$/MWh
$\boldsymbol{E_{45Y}}$	Lifetime of 45Y credits. Constrained by $\mathbf{2023} + \frac{E_{45Y}+S+C}{12} = \mathbf{2050}$ (see explanation below).	Months

[5] For example, to model yearly matching, the number of time steps in the optimization model is changed to 1. For monthly matching, only 12-time steps are required. For hourly matching, 8760 time steps are required.

$\mathcal{H}_{CE}[x]$	Cash-equivalent operator. Performs the conversion from nominal tax credits to cash-equivalent tax credits.	$
d_r	Discount rate.	
$LCOE$	Levelized cost of electricity	$/MWh
$CO_{2_{tax}}$	CO2 tax imposed by CBAM	$/Month
$CI_{SMR_{EU}}(T)$	European AP SMR carbon intensity.	Kg CO_{2eq}/kg H2
M_{H_2}	Mass flowrate of hydrogen	Tonnes per day
F_a	Availability factor	%
$CO_{2_{EUPrice}}$	Price for CBAM certificates.	$/tCO2
$R_{EU_{emissions}}$	Decay rate for EU AP SMR emissions intensity.	%
$L_{battery}$	Lifetime of battery system.	years
L_{wind}	Lifetime of wind farm turbines.	Years

Table E-2: Input values for section F.

Variables/Parameters	*Value*	*Source*
C_{f+v}^{wind}	52.22 $/MW/year	(Stehly et al., 2020)
$C_f^{battery}$	Uniform(6.16, 49.33) $/kW-year	(Cole & Frazier, 2019)
$C_v^{battery}$	Uniform(0,8.63) $/MWh	
L	480 months (40 years)	
S	0 months (year 2023) or 84 (year 2030)	Author assumption
C	36 months	
$48E$	Uniform(30%,40%)	IRA, 2022
$45Y(T)$	$1.5/MWh (when eligible)	
M_{H_2}	483 TPD	(Lewis et al., 2022)
F_a	90%	
$L_{battery}$	Uniform(13,20) years	(Cole & Frazier, 2019)
L_{wind}	20 years	(Stehly et al., 2020)
$CI_{SMR_{EU}}(T=0)$	8.82 $\frac{KgCO_{2e}}{KgH_2}$	(McDonald, 2023)

$R_{EU_{emissions}}$	1.4 %	(European Commission, 2023; Kakoulaki et al., 2021; McDonald, 2023)
$CO_{2_{EUPrice}}$	Uniform(35-100) $\frac{\$}{tCO_{2_e}}$	(McDonald, 2023)

E.1. Scenario B: Build-and-Own

To describe the changes we make to the baseline model (scenario A), we include a table with all the changes (Table E-3). We utilize some of the variables from the optimization problem and introduce some new variables in Table D-1. We define the AP plant time step to be $\boldsymbol{T} \in \boldsymbol{S} + \boldsymbol{C} + \boldsymbol{L}$ months**.** Let $\boldsymbol{\Gamma} = \boldsymbol{T} \bmod \mathbf{12}$ (so $\mathbf{0} \leq \boldsymbol{\Gamma} \leq \mathbf{11}$**)**. $\boldsymbol{\Gamma}$ is a useful transformation of $\boldsymbol{T}$ that allows us to extend the values of the optimization model from one year to 40 years of AP plant operation.

Table E-3: Changes to the baseline model to enable scenario B. All changes apply to the low-carbon technologies. AP SMR stays the same as the baseline.

Change	*Module Affected*	*Description*
Wind farm and battery storage CAPEX	CAPEX	The CAPEX of each technology is increased by $\boldsymbol{COST_{wind}} \times \boldsymbol{w} + \boldsymbol{COST_{battery}} \times \boldsymbol{b}$ except for AP SMR. The increased CAPEX is backpropagated to the rest of the CAPEX components.
Grid electricity costs	MDOPEX	Electricity costs from the grid are set to 0.
Wind farm and battery storage OPEX	MIOPEX	The electricity costs are replaced for the variable and fixed O&M costs of the hybrid farm and battery system. $$\boldsymbol{MIOPEX_{el}}(\boldsymbol{\Gamma}) = \boldsymbol{w} \times \frac{\boldsymbol{C_{f+v}^{wind}}}{\mathbf{12}} + [\boldsymbol{b} \times \frac{\mathbf{1000}}{\mathbf{12}}] \times \boldsymbol{C_f^{battery}} + \boldsymbol{d_{monthly}}(\boldsymbol{\Gamma}) \times \boldsymbol{C_v^{battery}}$$
$\boldsymbol{CI_{j \mid j \neq SMR_{Electricity}}}(\boldsymbol{T}) = \mathbf{0}$	Carbon Intensity	We assume the electricity generated from the hybrid wind farm is zero.
48E or 45Y credits	Tax Credits	The NPV model has added tax credits coming from IRA programs that support the hybrid wind farm system. The decision between 48E and 45Y is based on the NPV of each cash-equivalent tax credit. The formulation of the decision is long, so we describe it below in section E.1.1.
Selling surplus electricity	MDOPEX	Surplus electricity produced by the wind farm that is not stored can be sold to the grid at a larger price between the LCOE (see section E.2) of the wind farm and the market price: $$\boldsymbol{S_{el}}(\boldsymbol{T}) = \left[\boldsymbol{CF_{monthly}}(\boldsymbol{\Gamma}) * \boldsymbol{w} - \boldsymbol{w_{montly}}(\boldsymbol{\Gamma})\right] * \mathbf{max}[\mathbf{LCOE_{wind\ farm\ only}}, \boldsymbol{P_{Electricity}}(\boldsymbol{T}) * \mathbf{1000}]$$ So that $\boldsymbol{MDOPEX}(\boldsymbol{T})$ is increased by $\boldsymbol{S_{el}}(\boldsymbol{T})$**.**

Battery and wind farm have replacement costs	MIOPEX	Every $\boldsymbol{L_{battery}}$ and $\boldsymbol{L_{wind}}$ the uninstalled equipment cost of the wind and battery farm is incurred. We make this assumption as the project lifetime of wind farm and battery storage is shorter than AP[6].

E.1.1. Tax credits for scenario C.

The decision between 48E and 45Y is found below:

$$\max\left[\begin{matrix}\mathcal{H}_{CE}\left[\dfrac{\boldsymbol{48E}*\left(\boldsymbol{COST_{wind}}\times\boldsymbol{w}+\boldsymbol{COST_{battery}}\times\boldsymbol{b}\right)}{(\mathbf{1}+\boldsymbol{d_r})^{S+C}}\right], \\ \displaystyle\sum_{T=S+C}^{L+S+C}\mathcal{H}_{CE}\left[\dfrac{\boldsymbol{w}(\boldsymbol{\Gamma})\times\boldsymbol{45Y}(\boldsymbol{T})}{(\mathbf{1}+\boldsymbol{d_r})^{T-S}}\right]\end{matrix}\right] \tag{E.1}$$

$\boldsymbol{48E}$ credits are redeemed at the start of operation and are discounted to the present value. We assume $\boldsymbol{48E}$ credits also cover investments in the battery system.

$\boldsymbol{45Y}$ credits are spread out across time, hence the summation term. $\boldsymbol{45Y}(\boldsymbol{T}\,|\boldsymbol{S}+\boldsymbol{C}\leq\boldsymbol{T}\leq\boldsymbol{S}+\boldsymbol{C}+\boldsymbol{E_{45Y}})$ is non-zero and zero whenever $\boldsymbol{T}\notin\boldsymbol{S}+\boldsymbol{C}\leq\boldsymbol{T}\leq\boldsymbol{S}+\boldsymbol{C}+\boldsymbol{E_{45Y}}$. The lifetime of 45Y credits, $\boldsymbol{E_{45Y}}$, is determined to be when the grid emits 75% less than the 2022 grid. We first estimated this through $\frac{\boldsymbol{CI_{AP\,AEC}(T)}}{\boldsymbol{CI_{AP\,AEC}(T=0)}}=\mathbf{0.25}$ since $\frac{\boldsymbol{CI_{grid}(T)}}{\boldsymbol{CI_{grid}(T=0)}}\propto\frac{\boldsymbol{CI_{AP\,AEC}(T)}}{\boldsymbol{CI_{AP\,AEC}(T=0)}}$ because AP AEC's CI only varies with electricity. We find that grid emissions, according to the AEO2023, do not reach that level until after 2050 (EIA, 2023a). For simplicity, we assume $\mathbf{2023}+\frac{\boldsymbol{E_{45Y}+S+C}}{\mathbf{12}}=\mathbf{2050}$ so that $\boldsymbol{E_{45Y}}$ is a free variable that ensures $\boldsymbol{45Y}(\boldsymbol{T})$ is zero after 2050.

Once a tax credit program is chosen, the tax credits are added to the total tax credits. In the case of 48E, (E.2) is used. (E.3) is used when 45Y is larger than 48E.

$$\begin{matrix}\boldsymbol{Credits_{CE_{scenario\,C}}(T)}=\boldsymbol{Credits_{CE}(T)}+ \\ \boldsymbol{if}\left(\boldsymbol{T}=\boldsymbol{S}+\boldsymbol{C},\mathcal{H}_{CE}\left[\,\boldsymbol{48E}*\left(\boldsymbol{COST_{wind}}\times\boldsymbol{w}+\boldsymbol{COST_{battery}}\times\boldsymbol{b}\right)\,\right]\right)\end{matrix} \tag{E.2}$$

$$\boldsymbol{Credits_{CE_{scenario\,C}}(T)}=\boldsymbol{Credits_{CE}(T)}+\mathcal{H}_{CE}[\,\boldsymbol{w}(\boldsymbol{\Gamma})\times\boldsymbol{45Y}(\boldsymbol{T})] \tag{E.3}$$

E.2. Scenario C: Power Purchase Agreement (PPA)

The electricity price in scenario C becomes the LCOE of the hybrid wind farm and what we call the PPA price. The rest of this section describes how the PPA price was calculated. The PPA values can be found in Table E-5.

[6] The cost of the wind farm and the battery is the same cost as the start year. Hence, no technological improvements are taken into account. We adopt this assumption because the capacity factor data (and hence the optimization algorithm) is a function of the design parameters of the wind turbine. Relaxing this assumption brings about considerable computation barrriers and also has little effect on the PPA price (scenario C) or NPV (scenario B) because the replacement cost is heavily discounted. Consider that 75% of the value of the NPV or PPA price is derived from the first 13 years of performance. At 20 years, the replacement cost plays a small part in the economic performance.

The levelized cost method applied to the hybrid wind farm system is initially the same method as the baseline AP NPV model with an additional step to minimize the absolute value of the NPV by iterating through the levelized cost (LCOE or PPA price).

Table E-4: Changes to the baseline model to enable scenario C. All changes apply to the low-carbon technologies. AP SMR stays the same as the baseline.

Change	*Module Affected*	*Description*
Changes to the AP Model		
Change in the electricity price	MDOPEX	The new electricity price corresponds to the LCOE of the hybrid wind farm.
Changes to AP Model to derive the LCOE		
Every probabilistic value becomes the average value	All modules	
Heuristic factors for the CAPEX are no longer multiplied by a factor of $\frac{1}{\left(\frac{2717}{100}\right)^{0.6}}$. (see section C)	CAPEX	This scaling factor for the heuristics is not valid for the hybrid wind facility because the facility does not produce ammonia.
All OPEX costs are substituted for heuristics.	MIOPEX	The OPEX is becomes the $\boldsymbol{MIOPEX}(\boldsymbol{\Gamma})$. $$\boldsymbol{MIOPEX}(\boldsymbol{\Gamma}) = \boldsymbol{w} \times \frac{\boldsymbol{C_{f+v}^{wind}}}{\mathbf{12}} + [\boldsymbol{b} \times \frac{\mathbf{1000}}{\mathbf{12}}] \times \boldsymbol{C_f^{battery}} + \boldsymbol{d_{monthly}}(\boldsymbol{\Gamma}) \times \boldsymbol{C_v^{battery}}$$
Sales change from ammonia to electricity.	Sales	$$\boldsymbol{Sales}(\boldsymbol{\Gamma}) = [\boldsymbol{D_j} + [\boldsymbol{CF_{monthly}}(\boldsymbol{\Gamma}) * \boldsymbol{w} - \boldsymbol{w_{montly}}(\boldsymbol{\Gamma})]] * \boldsymbol{LCOE}$$
Only 48E or 45Y credits are considered	Tax Credits	48E or 45Y credits are applied using the same formulation as scenario C (see section E.1.1).
Instead of an NPV analysis, we use a levelized cost analysis.	DCF Model	We iterate the LCOE until the absolute value of the NPV is minimized. $$\arg \boldsymbol{LCOE} \min \sum_{T=0}^{L+S+C} \left\lvert \frac{\boldsymbol{CF_{LCOE}}(\boldsymbol{T})}{(\mathbf{1}+\boldsymbol{d_r})^{\boldsymbol{T-S}}} \right\rvert$$

Table E-5: PPA prices based on the LCOE model.

Time	**matching**	**Capacity factor**	**IRA?[A]**	$\boldsymbol{LCOE}\ [\frac{\mathbf{2023\$}}{\boldsymbol{MWh}}]$
2023	yearly	high	TRUE	46.22
2023	yearly	low	TRUE	101.18
2023	yearly	high	FALSE	71.06
2023	yearly	low	FALSE	156.00
2030	yearly	high	TRUE	26.59
2030	yearly	low	TRUE	66.23

2030	yearly	high	FALSE	48.50
2030	yearly	low	FALSE	88.15
2023	monthly	high	TRUE	46.29
2023	monthly	low	TRUE	101.19
2023	monthly	high	FALSE	71.13
2023	monthly	low	FALSE	156.01
2030	monthly	high	TRUE	26.64
2030	monthly	low	TRUE	66.27
2030	monthly	high	FALSE	48.56
2030	monthly	low	FALSE	88.20
2023	hourly	high	TRUE	113.77
2023	hourly	low	TRUE	262.28
2023	hourly	high	FALSE	138.61
2023	hourly	low	FALSE	408.65
2030	hourly	high	TRUE	83.31
2030	hourly	low	TRUE	115.40
2030	hourly	high	FALSE	105.22
2030	hourly	low	FALSE	173.74

[A] True means IRA subsidies were applied to the technologies (if they qualify). False means otherwise.

E.3. Carbon Border Adjustment Mechanism (CBAM)

The implementation of CBAM is a simple formula that measures the difference between the European AP SMR CI and the technology j. The magnitude of the difference is translated into the carbon tax below:

$$\boldsymbol{CO_{2_{tax}}} = (\boldsymbol{CI_{SMR_{EU}}(T)} - \boldsymbol{CI_j(T)}) \times \boldsymbol{M_{H_2}} \times \frac{\boldsymbol{365}}{\boldsymbol{12}} \times \boldsymbol{F_a} \times \boldsymbol{CO_{2_{EUPrice}}} \quad \text{(E.4)}$$

$$\boldsymbol{CI_{SMR_{EU}}(T)} = \boldsymbol{CI_{SMR_{EU}}(T=0)} * \left(\boldsymbol{1} - \boldsymbol{R_{EU_{emissions}}}\right)^{\frac{\boldsymbol{T}}{\boldsymbol{12}}} \quad \text{(E.5)}$$

We assume CBAM does not expire. The values for each parameter are found in Table E-1. We calibrated $\boldsymbol{R_{EU_{emissions}}}$ so that the EU AP SMR emissions in 2050 will match the predictions by the European commission and Kakoulaki et al. (2021). We chose an exponential decay type of relationship to show more pronounced emissions reductions early in the century and slower reductions towards the middle of the century.

F. Literature Review

This section briefly reviews the four AP technologies this report considers (Figure F-1**Error! Reference source not found.**). We start with the carbon-intensive, conventional AP SMR. Then, we describe AP SMR with Carbon Capture and Storage (AP CCS), followed by AP SMR with carbon-neutral biomass, as feedstock (AP BH2S). The last low-carbon technology pathway we considered for the AP is via Alkaline Electrolysis (AP AEC). Additionally, we include a comparison of each AP technology's technical advantages and disadvantages.

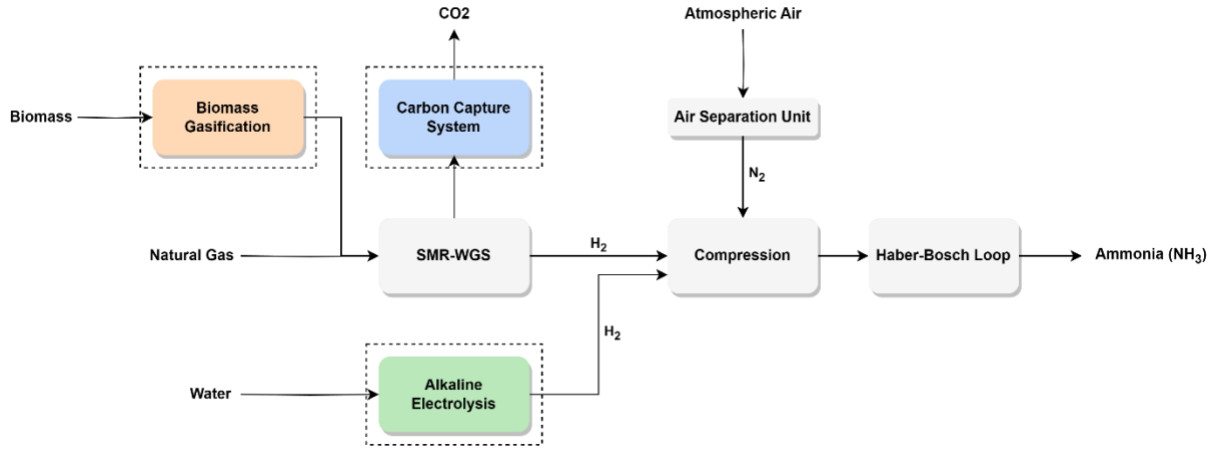

Figure F-1: Technology pathways analyzed in this report.

F.1. AP through Steam Methane Reforming (AP Baseline)

The common denominator across all technologies is the notable Haber-Bosch (HB) process – a chemical process by which pure sources of hydrogen (H_2) and nitrogen (N_2) gases combine to form ammonia (NH_3). The source of N_2 is separated from the air with an air separation unit (ASU), as air is 78% N_2 by volume. For H_2, natural gas (NG) is the most prominent source (78% of global AP) – although coal is also common (22%) (EIA, 2021). NG is chemically treated to obtain pure H_2 for the HB process selectively. Specifically, the chemical treatment for hydrogen production has three major steps (Amhamed et al., 2022; Appl, 1999; IRENA & AEA, 2022; MacFarlane et al., 2020):

1. NG is cleaned of impurities such as sulfur (Kim et al., 2021).
2. The NG is mixed with steam and reacted in several heated vessels – the first reaction is called steam-methane reforming (SMR), and the second is the water-gas shift (WGS) reaction. The resulting chemicals from these reactions are methane, CO_2, and H_2.
3. H_2 is separated from CO_2 and methane in a pressure-swing absorption unit (PSA). The pure H_2 product is sent to the HB process. The remaining methane and CO_2 heat the SMR vessel through combustion. Finally, the combusted gas is emitted into the environment through the plant's stack.

The H_2 from the HP process and the N_2 from the ASU must be compressed because the HB process requires extreme pressures and temperatures. The compression of H_2 and N_2 is the most energy-intensive step in AP. The source of energy for compression varies across technologies (see §2.5)

The typical AP SMR plant produces 500 to 3000 metric MTs per day (TPD) of NH_3 (Amhamed et al., 2022; IEA, 2021). The IEA reports that the break-even AP SMR ammonia price ranges from approximately $300 to $600 per ton of NH3, whereas the market price is between $200 and $750 in 2021 (IEA, 2021). Natural gas price constitutes 30% of the levelized cost of

ammonia (LCOA) as it is needed for hydrogen production and heating (Appl, 1999; Maxwell, 2012; Zhang et al., 2020). Therefore, a strong correlation between natural gas and ammonia markets exists. The remaining cost is attributed primarily to capital expenditure (CAPEX) and the rest to operational expenditure (OPEX) (Appl, 1999; Maxwell, 2012).

F.2. AP SMR with a Carbon Capture System (AP CCS)

The state-of-the-art CCS technologies are amine-based carbon sequestration units operated commercially for direct air or point-source capture[7]. This CCS technology operates by mixing CO_2-rich gases with water and amine solution to dissolve the CO_2 in the solvent. The CO_2-rich solvent can be stripped of the CO_2 by heating – effectively regenerating the solvent and obtaining pure CO_2 gas for transportation and storage. CCS systems can capture up to 95% of the CO_2 within the AP plant at an additional electric energy penalty cost relative to AP SMR. A report by the DOE comparing hydrogen production via SMR with and without CCS found that H_2 SMR required 0.65 kWh/Kg H_2 of electricity, while H_2 SMR with CCS required 2.04 kWh/Kg H_2 H_2 (Lewis et al., 2022).

F.3. AP SMR with a Biomass-derived feedstock (AP BH2S)

The natural gas feedstock of AP SMR can be substituted with biomass. Hydrogen production with a biomass feedstock utilizes the organic compounds in the biomass to generate small gaseous molecules (i.e., CH_4, C_2H_4, CO, CO_2, H_2, N_2, etc.) through a process known as gasification. These molecules are further processed into H_2 and CO_2 through the conventional SMR-WGS steps (Arora et al., 2016, 2017; Tock et al., 2013; Tunå et al., 2014). According to Spath et al., the organic molecules are converted to small molecules in a separate tar reformer before the SMR to pre-treat the syngas for sulfur contaminants and avoid char formation – although the goal design would be to perform tar reforming and SMR in the same vessel (Spath et al., 2005).

Biomass feedstocks are effectively net-zero, as the carbon emitted by biomass comes from the atmospheric CO_2 fixated into plants through photosynthesis. However, the electric energy requirements to process the biomass into usable NG-like synthesis gas are in the ballpark of AP CCS (Lewis et al., 2022; Spath et al., 2005). Hence, significant and possibly IRA-disqualifying indirect emissions of AP BH2S may be a fault of a carbon-intensive electric source (i.e., the electric grid) (EIA, 2023a).

F.4. AP via Alkaline Electrolysis (AP AEC)

The most abundant source of hydrogen is water. Water contains zero carbon and can be electrolyzed to produce pure hydrogen and oxygen gas. The advantage of electrolysis is that it is modular and suitable for decentralized systems (Böhm et al., 2020; Sousa et al., 2022). The current competing technologies are alkaline water electrolysis (AEC), proton exchange membrane electrolysis (PEM), and solid oxide electrolysis (SOE) (Böhm et al., 2020; dos Santos et al., 2017; Proost, 2017; Schmidt et al., 2017).

AEC is the most competitive technology as it has a high lifetime (60,000-90,000 hours (h)) and a low cost (1300-500 $/kW) when compared to PEM (20,000-90,000h and 2000-800 $/kW) (Schmidt et al., 2017). SOE stacks have the highest cost among all technologies (5000-1500 $/kW) and the shortest lifetime (<20,000h) as they are still at the laboratory stage (Schmidt et al., 2017). Nevertheless, SOE stacks are expected to experience the most significant cost reductions from deployment and R&D (Lee et al., 2021; Schmidt et al., 2017). AP AEC forms a small part of AP in general (<0.02 Mt in 2021) (Böhm et al., 2020; IRENA & AEA, 2022). AEC pathways and other electrolysis technologies expect cost reductions of 0-24% from R&D and 17-30% from production scale-up (Schmidt et al., 2017).

[7] In this report, CCS refers to Methyl diethanolamine (MDA) solvent-based carbon capture units.

While electrolytic pathways mitigate emissions by ensuring a zero-carbon feedstock, the additional electric energy demand can be higher (Singh et al., 2019). Gomez and colleagues identified that H2 electrolysis required 50-60 kWh/kg H_2 versus 0.65 kWh/kg H_2 for SMR (Gomez et al., 2020; Lewis et al., 2022). The additional electricity usage renders electrolytic hydrogen production to be non-zero because of the indirect emissions of the grid and construction materials. Simons and Bauer estimate solar-powered electrolysis at 3 kg CO_2 eq/kg H_2 and wind at 2 kg CO_2 eq/kg H_2 due to the indirect emissions of the construction materials for wind and solar alone (Simons et al., 2011).

F.5. Economic and environmental comparison of AP across the literature.

The most often used and preferred method in the literature to compare economic performance of low carbon hydrogen and ammonia is the levelized cost approach (LCOH and LCOA) (Arora et al., 2016, 2017; Campion et al., 2022; del Pozo & Cloete, 2022; Gomez et al., 2020; Guerra et al., 2020; Lee et al., 2021; Lewis et al., 2022; Osman et al., 2020; K. H. R. Rouwenhorst et al., 2019; Sánchez et al., 2019; Sousa et al., 2022; Tock et al., 2013; G. Wang et al., 2020a; Zhang et al., 2020). The LCOA, while pertinent in numerous instances, is primarily focused on the production cost side of the equation, potentially overlooking the IRA's significant dynamics, which influence the revenue side.

This revenue-side influence, particularly concerning income taxes, is outside the scope of the LCOA, necessitating assumptions that could potentially overstate outcomes[8]. For instance, Jenkins et al. (2023) implicitly assumed all tax credits equal $1 US dollar by awarding full credit value to their levelized cost analysis. This approach may lead to overestimations, particularly regarding policy support for low-profit, riskier, low-carbon technologies that heavily rely on a tax credit market. Consequently, this study adopts the NPV approach, offering a more comprehensive and nuanced perspective better suited to capturing the real-world effects of income tax credit-based policies like the IRA.

Regarding the electric energy intensity of AP, compressing the gas out of the HP and ASU systems before the HB loop is known to be a highly energy-intensive step. Hence, using surplus energy from other parts of the process is a critical step that may sometimes drive AP SMR to generate electricity (IEAGHG, 2017). This energy integration step is essential in determining the relative OPEX between AP SMR and low-carbon technologies. Some technologies lack surplus energy to power the compression and need to purchase energy from the grid.

In general, AP SMR may have surplus energy to power the entire compression load, and hence, it uses the least amount of grid electricity (IEAGHG, 2017; Lewis et al., 2022). AP CCS does not have surplus energy and uses grid electricity (IEAGHG, 2017; Lewis et al., 2022). AP BH2S does have surplus energy for one compression process but has two in total – hence using around the same amount of grid electricity as AP CCS (Spath et al., 2005). Finally, AP AEC needs an order of magnitude larger amount of electricity for hydrogen production. It does not have surplus energy for compression – making it the most electrically energy-intensive process in the portfolio (Gomez et al., 2020). Regarding total energy efficiency, AP AEC is the least efficient, followed by BH2S and CCS. AP SMR is the most energy-efficient pathway (del Pozo & Cloete, 2022; Smith et al., 2020; Spath et al., 2005; Tock et al., 2013).

[8] The LCOA's effective income tax rate skews towards 0% as the revenues generated are only sufficient to offset the costs. With no income tax to abate, this framework's dependence on selling tax credits invites the risk of incorporating potentially oversimplifying assumptions. This issue becomes particularly notable under conditions of an unpredictable tax credit market.

In terms of economic cost assessment, large-scale AP SMR plants, with capacities above 2000 TPD of ammonia, can have capital expenditure (CAPEX) ranging from $500M ($250k/TPD NH3) to $1800M ($900k/TPD NH3) and operating expenditure (OPEX) ranging from $180 to $500 per ton of NH3 (IEA, 2021; Maxwell, 2012; Pfromm, 2017). For AP CCS at an 88.2% capture rate, the CAPEX is estimated to be between $298k/TPD NH3 and $275k/TPD NH3, with an OPEX of €280/Ton NH3 (del Pozo & Cloete, 2022). On the other hand, AP BH2S costs have been studied at scales of 73 to 1187 TPD NH3. Arora et al. (2017) provided a detailed process model for biomass gasification at 73.5 TPD NH3. They noted that the CAPEX and OPEX of biomass gasification are between $170k to $175k/TPD NH3 and $705 to $722/ton NH3, respectively.

Although specific cost data for AP AEC was not easily found in the literature, it is likely to have similar or higher costs than AP CCS and AP BH2S, depending on variable factors such as electricity costs (OPEX-related) and electrode stack costs (CAPEX-related), which are highly uncertain variables (Sousa et al., 2022). AP AEC is the pathway expected to reduce cost due to modularity (Schmidt et al., 2017). AP CCS is expected to remain at a similar cost level –hence only seen as a transitory technology for decarbonization (MacFarlane et al., 2020). AP BH2S, on the other hand, presents significant uncertainties regarding its cost and feedstock availability (Sánchez et al., 2019; Tock et al., 2013; Tunå et al., 2014).

On the environmental front, life cycle assessments (LCA) of AP SMR produce variable results involving the emissions intensity of ammonia production. The cradle-to-gate equivalent CO_2 emissions of AP SMR varied by 10 to 15% from the average across studies (Bicer et al., 2016; Bicer & Dincer, 2017; Liu et al., 2020). For example, Bicer and colleagues measured the emissions intensity for AP SMR to be 1.6 kg of equivalent CO2 emissions (kgCO2e) per kg of NH3 with a plant-wide scope, while ARPA-E reported a value of 2.55 kgCO2e/kgNH3 for a cradle-to-gate analysis using the GREET model (Bicer et al., 2016; Bicer & Dincer, 2017). Liu and colleagues reported emissions intensities of around 1.8 kgCO2e/kgNH3 for a cradle-to-gate scope (Liu et al., 2020). Young and colleagues found that CCS reduced cradle-to-gate CO2e emissions by 69% (B. Young et al., 2019).

The DOE report on hydrogen production via SMR with CCS found similar results at a 61% reduction in cradle-to-gate CO2e intensity (Lewis et al., 2022). The average CO2e intensity of AP SMR across four studies is approximately 11.7 kgCO2e/kgH2 (1.99 kgCO2e/kgNH3[9]) (Bicer et al., 2016; Bicer & Dincer, 2017; Liu et al., 2020) – Please note that reductions by 61-69% qualify AP SMR with CCS for significant 45Q carbon sequestration credits under IRA (Bauer et al., 2022; Lewis et al., 2022).

AP through BH2S has been considered a viable alternative to ammonia production as it is a zero-carbon fuel (Arora et al., 2016, 2017; Gilbert et al., 2014). Gilbert and colleagues show that biomass reduces cradle-to-gate emissions to 0.7 kg CO2e/kg NH3 (3.95 kg CO2e/kg H2) from a 1.9 kg CO2e/kg NH3 (10.7 kg CO2e/kg H2) natural gas AP SMR baseline (Gilbert et al., 2014). The environmental performance of AP w/ BH2S has also been shown to decrease with increasing scale at varying proportions depending on the type of biomass. Arora et al. (2017) display results indicating the inverse relationship between decreasing life-cycle emissions and scale-up cost reductions (Arora et al., 2017).

[9] Hydrogen is approximately 17% of NH3 by mass. Hence, carbon intensity values on a per-NH3 or H2 unit are interchangeable. Regardless of basis units, ammonia processes will be more carbon intensive as there is more processing than hydrogen production.

While AP AEC pathways mitigate emissions by ensuring a zero-carbon feedstock, the additional indirect electric energy emissions can be higher. The estimated potential emissions intensity of AP AEC can range between 4.4-2.2 kg CO2e/kgH2. Simons and Bauer estimate solar-powered electrolysis at 3 kg CO2e/kgH2 and wind at 2 kgCO2e/kgH2 due to the indirect emissions of the construction materials for wind and solar (Simons et al., 2011). Borole and Greig estimated wind-powered electrolysis at 0.97 kgCO2e/kgH2, and Valente et al. estimated 0.3 kgCO2e/kgH2 (Borole & Greig, 2019; Valente et al., 2020). Liu and colleagues estimated the emissions intensity of N2 production and the Haber-Bosch to be 0.3 kgCO2e/kgH2 and 0.9 kg CO2e/kgH2, respectively (Liu et al., 2020). By adding Liu et al.'s estimates to the results, the estimated potential emissions intensity of AP AEC can range between 4.4-2.2 kg CO2 eq/kg H2.

In essence, AP CCS and AP BH2S are effective strategies for significantly reducing the carbon emissions associated with AP SMR. Despite this, AP CCS is inherently limited by a capture rate that falls short of 100%, leading to unavoidable residual emissions. In contrast, AP BH2S holds the potential for near-net-zero emissions at the risk of limited feedstock supplies and quality. Alternatively, AP AEC can attain net-zero emissions, provided that the emissions linked to the production of materials are disregarded, especially in scenarios where the power generation is green.

F.6. Haber-Bosch Flexibility

F.6.1. HB Flexibility in Literature

The maximum flexibility of the HB loop varies widely between sources, ranging from 10% of nominal capacity (Ostuni & Zardi, 2011) to nearly 80% (Verleysen et al., 2023), with most estimates being concentrated around the 40% level. This wide variance can be attributed to a range of underlying assumptions made by various authors; Verleysen et al. conservatively estimate a flexibility of 78.7% of maximum capacity while optimizing system performance under realistic operational constraints. They also observe a significant 76.2% decrease in mean AP for a 9.33% increase in flexibility.

Another study by Cheema and Krewer found through physicochemical modeling that by reducing the H2-N2 ratio in the feed, H2 consumption can be reduced by 67% with a consequential 17% increase in recycle load (2018). Cocon conducted a technical design optimization of an HB reactor while fluctuating the feed stream composition (H2:N2) from 3:1 to 1.31:2.69 over a 24 minute simulation. No substantive comments were made on the economic implications of implementing such a reactor (Cocon 2020).

Armijo and Philibert outline a standard flexibility case through interviews with manufacturers where HB flexibility is 40% of nominal capacity with a ramp rate of +/-20% of nominal capacity per hour (2020). Further, they conclude that this ramp rate is more than sufficient to not be a limiting factor, which is corroborated by Wang et al. (2023). Another first-principle-based analysis by Lazouski et al. finds that the energy efficiency of the ammonia production reaction must be greater than 32%, and energy efficiencies below 30% dramatically increase energy costs (2022).

These studies primarily examine the technical capabilities of HB while forgoing economic feasibility evaluation. Analyses based on cost-effectiveness yield a smaller operable capacity range; a study by Onodera et al. found a cost-optimized capacity factor for HB of 73% as part of a larger flexible AP system. Further, they found that a flexible production capacity was economically preferable to a battery buffer storage system (2023).

Allowing for flexible HB operation involves weighing the costs and benefits of reduced electricity matching requirements against the obvious reduced production, but also the increased risk of damaging process equipment under non optimal operating conditions (Ostuni & Zardi, 2011). Flexibility in HB operation is a prominent cost driver as the CAPEX associated with supplemental renewable energy infrastructure is significantly larger than that of ammonia production or generation of hydrogen. Oftentimes, the minimum load of a flexible HB process is more impactful on overall process system costs than HB CAPEX itself given the impact of minimum load on sizing of supplemental power equipment (Wang et al., 2023). It was determined that a minimum HB load decrease from 60% of nominal to 10% supported by a hybrid renewable energy system (wind and PV) resulted in a 7.1% and 3.9% decrease in LCOA in two Australian locations for which simulations were conducted (Wang et al., 2023).

F.6.2. Applications of HB Flexibility in Industry

While flexibility in an HB loop is possible, research into its practical implementation and cost effectiveness is in its early stages. The breadth of literature suggests the extent to which the HB process can be operated flexibly depends on the lens through which analysis is conducted. Multiple technical analyses and patents purport HB operating ranges down to 10% of nominal capacity with ramp rates of +- 20%/hr (Ostundi & Zardi, 2011). That said, economic analyses find optimal performance within significantly more stringent constraints (between 70 and 80% capacity) (Onodera et al., 2023; Verleysen et al., 2023).

There are groups working to better understand the state of flexible HB technology through more pragmatic implementation. A report for the British government introduces the Ammonia Synthesis Plant from Intermittent Renewable Energy (ASPIRE) project. This project proposes the use of seven synthesis reactors in parallel which can individually be powered on and off to achieve flexibility of down to 5% of maximum capacity (0.5MW to 10MW), storing excess thermal energy to keep idle reactors up to operating temperature (Davenne et al., 2022). They also find that flexible HB design is preferable to either energy or hydrogen storage units due to significantly reduced CAPEX. They claim that the technology for this flexible design is commercially available, but even their model plant is still in the planning stages.

The Danish green energy company Topsoe plans to pilot a 25 MT per day ammonia plant with 10% to 100% flexibility in early 2024, with further plans to upscale to 1800 MT per day by 2025 (K. Rouwenhorst, 2023). Even when process economics are considered, there is little research into how incorporation of flexibility into a HB process will affect CAPEX, making the overall value of such a development difficult to estimate. Even Topsoe acknowledges cost optimization has not been performed on the pilot plant due to small scale process economics not being reflective of full scale. With the IRA expiring in 2035, there are economic incentives to utilize mature, available technologies to maximize the benefits of these policies.

G. Validation

G.1. Convergence of Monte Carlo Results

This study examined the variability of NPV values across total Monte Carlo simulations for SMR, CCS, BH2S, and AEC. Our primary objective was to evaluate the robustness of NPV values as

they evolve with an increasing number of simulations, thereby providing insights into their stability in response to varying levels of simulation.

For each technology, scenario, and year, we performed simulations comprising 500, 1000, 2000, 4000, and 8000 iterations (see annexed Excel file named ***AP_NE_Convergence_On_NPV.xlsx***). We gathered statistical data during these simulations encompassing maximum, minimum, P95, P5, mean, and median values. We chose to run the model at 4,000 simulations for data collection for the reasons outlined herein.

At the outset of our analysis, we observed noteworthy fluctuations in NPV values during the initial 300 runs, indicating potential uncertainty in the early iterations. However, beyond the threshold of approximately 2000 runs, the NPV values gradually stabilized, with fluctuations diminishing significantly. Across most scenarios, a discernible convergence trend emerged after the 2000-run mark, suggesting that further iterations had a limited impact on the NPV values. We found 4,000 to be the right balance between ensuring convergence and maximizing computational tractability.

G.2. Comparison of SMR baseline to IEA

The IEA shows a detailed chart of a levelized cost analysis they performed on various technologies. To validate our techno-economic methodology, we compare our AP SMR levelized cost to the AP SMR LCOA reported by the IEA (Figure 1.6, page 40) to the deterministic levelized cost of this study (IEA, 2021).

We use the sensitivity inputs for natural gas and electricity the IEA uses to obtain the range of LCOAs (see Table G-1). The IEA assumes a higher capacity factor (95%) and smaller CAPEX heuristics – hence, having a reduced CAPEX compared to this study[10]. The figure below illustrates the comparison (Figure G-1). They assume a smaller discount rate of 8% (we use 9.3%) and a shorter operating lifetime (25 years versus 40 years). Therefore, their TEA is less sensitive to changes in the OPEX because the operating lifetime is much smaller (although the difference in discount rates may reduce this difference).

Table G-1: Comparison of inputs of IEA versus this study.

Inputs	**IEA, 2021**	**This study**
Electricity (cents/kWh)	1.0 – 10	6.3
Natural gas ($/MMBtu)	2.8 – 7.765	2
Availability (%time)	95	90
Discount factor (%$)	8	9.3
CAPEX heuristics (%PEC)[A]	+70	>+100
Lifetime (years)	25	40

[A] PEC = purchased equipment cost

Notes: For comparisons with the IEA's levelized cost, the inputs shown here differ from the baseline models we show in the previous SI sections. Here, we set the electricity and natural gas baseline values to the 2020 prices to align with IEA's assumptions.

[10] They increase their equipment costs by 70% to estimate the CAPEX for "engineering, procurement, and construction costs" (IEA, 2021). Our estimates increase the equipment costs well over 100% to estimate the additional costs of more cost factors such as site improvements, contingency, legal expenses, and contractor fees, among others (see section B).

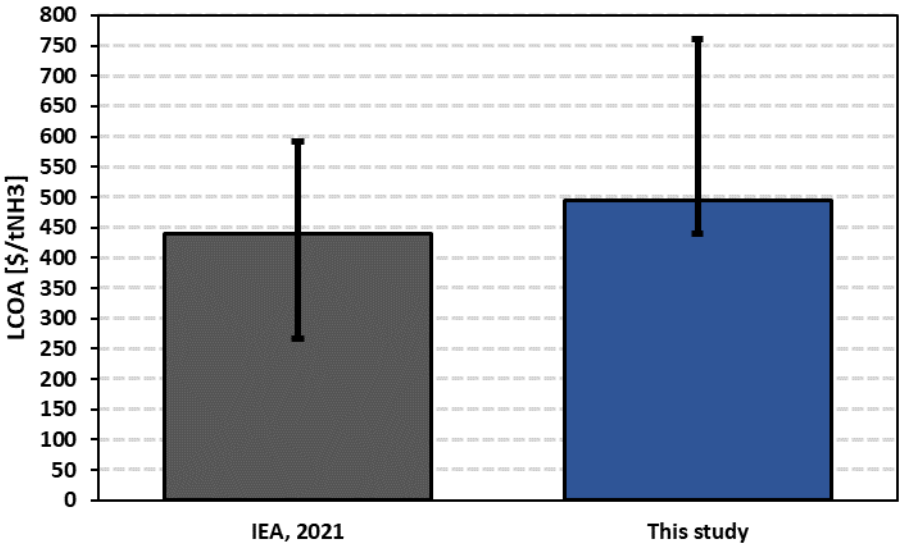

Figure G-1: This study's deterministic LCOA compared to IEA's *Ammonia Technology Roadmap* report (IEA, 2021).

The deterministic LCOA is computed by setting the NPV to zero (similar to the LCOE, see SI D). The deterministic NPV is calculated by taking the average of all probabilistic inputs. The high and low error bars represent instances when the model takes the maximum and minimum probabilistic values, respectively. Furthermore, in the minimum and maximum scenarios, we take on the electricity and natural gas values that the IEA uses (see Table G-1).

In conclusion, the values we obtain are close to those of the IEA, considering the large differences across input values. Our plant model is more sensitive to natural gas, ammonia, and electricity markets (denoted as $\boldsymbol{P_i(T)}$ in SI B) than the IEA's AP SMR. Moreover, we conservatively estimate the CAPEX with additional cost factors, contributing to the upward shift in LCOA from the IEA's LCOA.

G.3. Sensitivity Analysis of Inputs

Ensuring the quality of our TEA through a sensitivity analysis will help us determine if directional changes in the inputs result in economically sensible shifts in the NPV of the technologies. We include an Excel file named ***AP_NE_Sensitivities.xlsx,*** which shows the difference in NPV [$/tNH3] between the deterministic baseline and the sensitivity analysis. The "input" column depicts the change in the input variables in the high and low scenarios. The sensitivities are ranked in descending order by the sum of the NPV shifts across technologies**.**

We set the bounds of the sensitivity analysis to be the distribution limits for probabilistic values and +/-20% for deterministic and composite values. Composite values are values that sit in between the outputs and inputs. For example, the OPEX is a composite value because it is not an input or an output.

There are values in the file that do not contain the input bounds for the sensitivity analysis – namely, "AEC Stack Cost" and "Wind Turbine CAPEX". This is because the bounds of these values change over time. To find the bounds, refer to the 2023 and 2030 costs we set for these costs in SI B and D.

In the deterministic version of the AP model, we handled commodity prices differently from the probabilistic counterpart. We set the standard deviation of the GBM module to 0 to express linear changes in commodity prices across time. This slightly affects the sensitivity analysis results (see section G.4.3)

G.3.1. CAPEX-related Sensitivities

We consider the AEC CAPEX, the total CAPEX, and the wind CAPEX for the sensitivity analysis. We do not consider the battery CAPEX since monthly matching has no allocated battery capacity.

For validation, the wind and battery CAPEX have the same sign (negative) and are part of the same equation in the Python model. Hence, they behave similarly in the hourly matching sensitivity (where battery capacity is allocated).

Varying the overall CAPEX (composite value) by +/-20% has little effect on the NPV in scenario A. Less than $1/tNH3 was recorded, so it was rounded to 0, as such a difference is statistically insignificant. In scenario B, the CAPEX disproportionately affects the AP CCS, AP BH2S, and AP AEC NPVs relative to AP SMR. This is caused by the additional cost of the hybrid wind farm, which increases the CAPEX for the low-carbon technologies. Consequently, changes by +/-20% in the low-carbon CAPEX will also vary the CAPEX of the hybrid wind farm – thereby becoming a more sensitive parameter. AP AEC is the most sensitive because its CAPEX is the biggest (see **AP_NE_CAPEX.xlsx**). In scenario C, the CAPEX sensitivity regresses to scenario A sensitivity because the only difference between scenario A and scenario C is the OPEX.

This parameter is more sensitive than the CAPEX for the AEC stack CAPEX. This is because the range of variation, in terms of percentage points, is +/- 33%. Remember that the AEC stack CAPEX is a probabilistic parameter that varies according to its bounds.

G.4. OPEX-related Sensitivites

We consider the process related OPEX (MI OPEX) and market dependent commodity prices (electricity and natural gas) for monthly matching.

G.4.1. Process related OPEX

The process related OPEX is the largest in scenario B because of the O&M costs of the hybrid wind farm for low-carbon technologies and looks correlated with the electricity price. AP SMR only experiences a shift of $6/tNH3 when decreasing the process related OPEX by 20%. Meanwhile AP AEC experiences a change of $65/tNH3 with the same change. This is due to the scale of the hybrid wind fam, which incurs severe O&M costs. Note that the hybrid wind farm scale is directly proportional to the electricity demand of the AP technology. AP CCS and AP BH2S sit in between AP SMR and AP AEC with changes of $19/tNH3 and $25/tNH3 in scenario B, respectively.

In scenarios A and C, the process OPEX is similar for all technologies. This is because the electricity price is not part of the process OPEX – the electricity price being the only difference between scenarios A and C in terms of OPEX. Hence, the cost drivers cause the same directional change. This change is less than scenario B. AP SMR, AP CCS, AP BH2S, and AP AEC only incur a $6/tNH3, $8/tNH3, $15/tNH3, and $9/tNH3 with a 20% decrease in the process OPEX, respectively.

G.4.2. Market commodities

Natural gas and electricity prices were found to be significant cost drivers of the AP process. In the probabilistic model, we enforce a correlation between ammonia and natural gas prices through a bivariate distribution. In the deterministic model, we take the average markup from natural gas to ammonia prices, and make the ammonia price dependent on the product of the natural gas price and the markup. We do this to capture the hedging effect we see in the probabilistic model.

The natural gas price along drives a large part of the NPV of AP SMR and AP CCS across all scenarios. We set a range of prices by taking the minimum and maximum natural gas prices from December 2014 until January 2023 (EIA, 2023b). Changing the natural gas price results in hedging as we see when the price is set at $2.58/MMBtu, the NPV of AP SMR and AP CCS decrease by -$42/tNH3 and -$48/tNH3 while AP BH2S and AP AEC decrease by -$75/tNH3 and -$84/tNH3. On the high sensitivity ($9.95/MMBtu), the NPV of AP SMR and AP CCS decrease by $90/tNH3 and $91/tNH3 while AP BH2S and AP AEC decrease by $100/tNH3 and $109/tNH3. We see the hedging effects result in approximately twice the loss for non-hedged technologies (AP BH2S and AP AEC) when natural gas prices reduce (and hence ammonia prices). On the other hand, the potential gain from not hedging results in 21% higher increase in NPV for BH2S and 11$ for AP AEC.

The markup between NH3 and natural gas was also varied. The low is 58.96 $NH3/$NG and the high is 204 $NH3/$NG. Changing the markup directly changes the ammonia price without affecting the natural gas price. Consequently, both AP SMR and AP CCS increase by $51/tNH3 when the markup is high. Similarly, AP BH2S and AP AEC increase by $52/tNH3 and $62/tNH3. On the other hand, low markup results in a loss of -$76/tNH3, -$86/tNH3, -$85/tNH3, and -$94/tNH3 for AP SMR, AP CCS, AP BH2S, and AP AEC, respectively. These results vary slightly across scenarios due to tax-credit and profitability effects (see section I). Nevertheless, the general trend holds.

The electricity price is one of the foundation of the NPV difference between AP SMR and the low-carbon technologies (specially AP AEC). In scenario A, the electricity price affected AP SMR, AP CCS, and AP BH2S less than their feedstock cost – specifically by +/- $1/tNH3, $3/tNH3, and $3/tNH3. The effects of biomass feedstock on BH2S were + $14/tNH3 and -$15/tNH3 for a decrease to $50.68/dry tonne and an increase to $118.24/dry tonne, respectively. Meanwhile, AP AEC uses the electricity to drive the energy input into the hydrogen product (given the delta in thermodynamic energy states of water and hydrogen gas), which results in a dramatic sensitivity of +/- $29/tNH3 for a +/- 20% change in the electricity price in scenario A.

In scenario B, the electricity cost sensitivity goes to zero for the low-carbon technologies and remains at the same level for AP SMR. This is because the electricity costs are shifted to the hybrid wind farm CAPEX and O&M costs.

In scenario C, the electricity cost sensitivities are the same as scenario A. Although AP AEC shows slightly less sensitivity at +/- $28/tNH3 – which can be considered negligible.

G.4.3. Policy Sensitivities

We consider sensitivity of +/-20% for all programs except 48E, which was varied between 30% and 40% ITC. In scenario A, 45V credits are the only sensitive parameter. AP CCS can claim 45Q – however, this choice is suboptimal. In scenario A, AP CCS and AP BH2S

are the only technologies receiving tax credits. Changing 45V credits by +20% results in a change of $4/tNH3 and $3/tNH3 for AP CCS and AP BH2S, respectively.

In scenario B, 45V and 48E credits are the only sensitive parameters. 48E credits are always preferred over 45Y credits given that the return on energy per $ CAPEX invested in the wind farm is not high enough make 45Y credits desirable. We find that 45V credits have a symmetric and similar effect for all three low-carbon AP technologies. The variation is +/- $12/tNH3 for AP CCS, AP BH2S, and AP AEC. 48E credits are symmetrical around the high and low sensitivities but not across technologies. The high electricity demand of AP AEC increases the scale of the hybrid wind farm – thereby increasing the amount of 48E credits awarded to AP AEC. We see AP AEC net an increase in NPV of +/- $13/tNH3. AP CCS and AP BH2S only receive +/-$2/tNH3. Note that for the deterministic model we took the inputs as the average of the probabilistic ranges, hence the baseline value for 48E credits is 35% -- which is technically not possible given the step-wise nature of the 48E program (either 30% or 40%). This discontinuity is expressed in the probabilistic model. If we were to set the 48E credits to 30%, then the sensitivity would be $0/tNH3 in the low scenario and twice the change in the high scenario.

In scenario C, 45V credits have the same effect on the NPV as in scenario B. In scenario C, all other credits are not sensitive because (i) the hybrid wind farm is not part of the system and (ii) 48Q credits are not preferable to 45V credits in the case of AP AEC – these two conditions leave only 45V credits.

G.4.4. Conclusions on validating sensitivities

We find sensical changes in the NPV when varying the inputs. First, cost side variables drive the prices down and revenue side variables drive prices up. Second, in areas related to asymmetric resource demand across technologies (i.e., electricity demand), we see unequal changes in the NPV per unit input. On the revenue side, we find the expected hedging that AP SMR and AP CCS have against ammonia and natural gas price movements. In cases where the carbon intensities are high, we see a decreased sensitivity in policy support – which is also expected. With these results we find confidence in the formulation of the model.

H. Additional Results

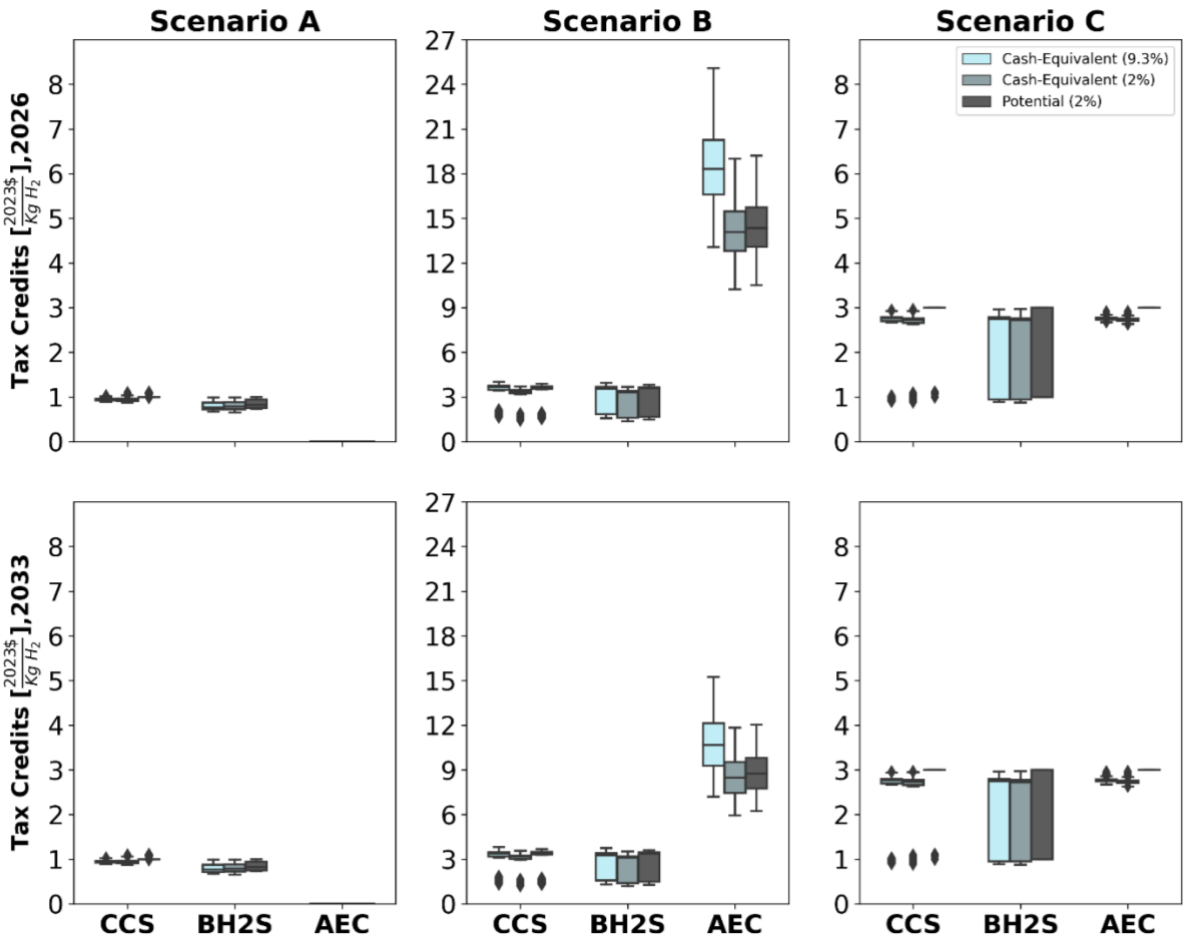

Figure H-1: Hourly matched total policy support in $/Kg H2. Notice scenario B charts have a y axis three times larger than scenarios A and B.

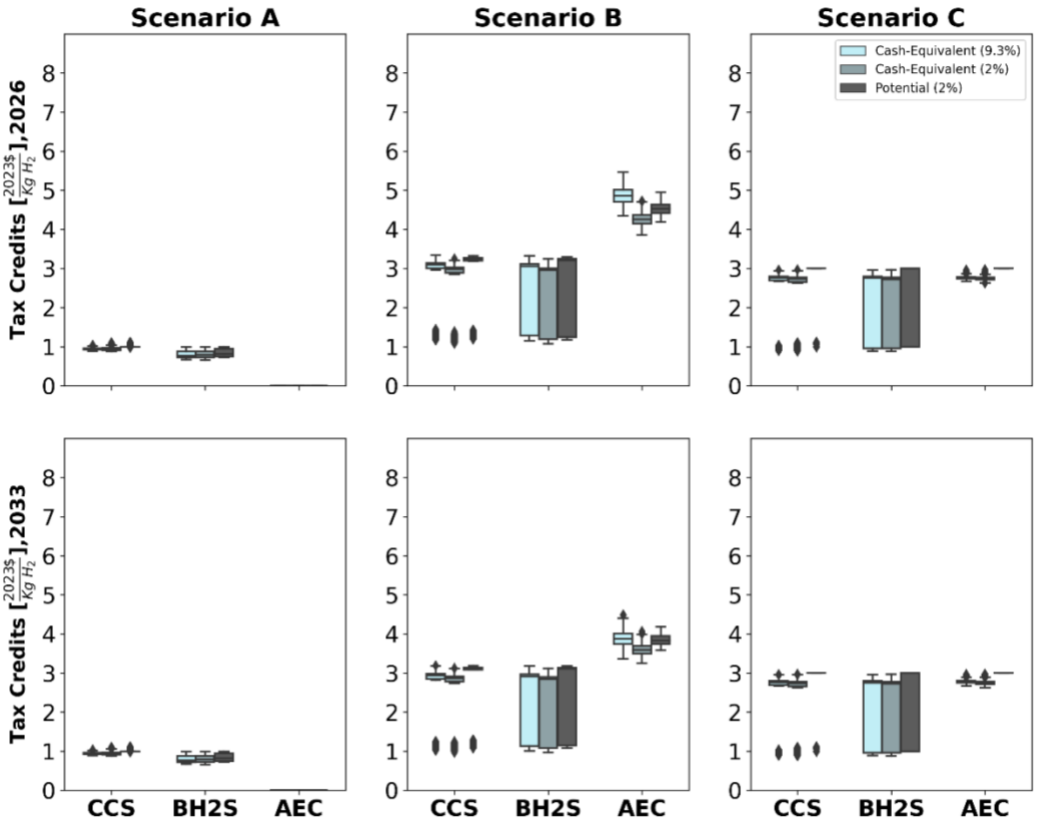

Figure H-2: Yearly matched total policy support in $/Kg H2.

Figure H-3: Mean electricity price over time. The GBM model collapses to a linear model across 4000 simulations.

I. References

Amhamed, A., Qarnain, S. S., Hewlett, S., Sodiq, A., Abdellatif, Y., Isaifan, R. J., & Alrebei, O. F. (2022). Ammonia Production Plants—A Review. *Fuels*. https://doi.org/10.3390/fuels3030026

Armijo, J., & Philibert, C. (2020). Flexible production of green hydrogen and ammonia from variable solar and wind energy: Case study of Chile and Argentina. *International Journal of Hydrogen Energy*. https://doi.org/10.1016/j.ijhydene.2019.11.028

Appl, M. (1999). Process Steps of Ammonia Production. In *ammonia* (pp. 65–176). https://doi.org/https://doi.org/10.1002/9783527613885.ch04

Arora, P., Hoadley, A., Mahajani, S. M., & Ganesh, A. (2017). Multi-objective optimization of biomass based ammonia production - Potential and perspective in different countries. Journal of Cleaner Production. https://doi.org/10.1016/j.jclepro.2017.01.148

Arora, P., Hoadley, A., Mahajani, S. M., & Ganesh, A. (2016). Small-Scale Ammonia Production from Biomass: A Techno-Enviro-Economic Perspective. Industrial & Engineering Chemistry Research. https://doi.org/10.1021/acs.iecr.5b04937

D'Alelio, D., Jiang, M., Langer, J., Lerner, N., Pan, E., & Puritz, J. (2022, May 16). *Current Challenges to Tax Equity (Part Three)*. Clean Energy Finance Forum.

Bauer, C., Treyer, K., Antonini, C., Bergerson, J., Gazzani, M., Gencer, E., Gibbins, J., Mazzotti, M., McCoy, S. T., McKenna, R., Pietzcker, R., Ravikumar, A. P., Romano, M. C., Ueckerdt, F., Vente, J., & van der Spek, M. (2022). On the climate impacts of blue hydrogen production. *Sustainable Energy and Fuels*, *6*(1). https://doi.org/10.1039/d1se01508g

Bartlett, J., & Krupnick, A. (2019). *Subsidizing Carbon Capture Utilization and Storage: Issues with 45Q*.

F. Barbir, A. Basile and T. N. Veziroglu. (2016) Compendium of Hydrogen Energy, Woodhead. Publishing, Elsevier, Amsterdam, Netherlands.

Bicer, Y., & Dincer, I. (2017). Life cycle assessment of nuclear-based hydrogen and ammonia production options: A comparative evaluation. *International Journal of Hydrogen Energy*. https://doi.org/10.1016/j.ijhydene.2017.02.002

Bicer, Y., Dincer, I., Zamfirescu, C., Vezina, G., & Raso, F. (2016). Comparative life cycle assessment of various ammonia production methods. *Journal of Cleaner Production*. https://doi.org/10.1016/j.jclepro.2016.07.023

Brasington, R. D., Haslback, J. L., Kuehn, N., Lewis, E., Pinkerton, L. L., Turner, M. J., Varghese, E., & Woods, M. (2011). Cost and Performance Baseline for Fossil Energy Plants - Volume 2: Coal to Synthetic Natural Gas and Ammonia. https://doi.org/10.2172/1515254

Brauns, J., & Turek, T. (2020). Alkaline water electrolysis powered by renewable energy: A review. In *Processes* (Vol. 8, Issue 2). https://doi.org/10.3390/pr8020248

Böhm, H., Zauner, A., Rosenfeld, D. C., & Tichler, R. (2020). Projecting cost development for future large-scale power-to-gas implementations by scaling effects. *Applied Energy*. https://doi.org/10.1016/j.apenergy.2020.114780

Borole, A. P., & Greig, A. L. (2019). Life-cycle Assessment and Systems Analysis of Hydrogen Production. *Biohydrogen*. https://doi.org/10.1016/b978-0-444-64203-5.00020-4

Boston Consulting Group. Green Hydrogen: An assessment of near-term power matching requirements. (2023).

Bistline, J., Blanford, G., Brown, M., Burtraw, D., Domeshek, M., Farbes, J., Fawcett, A., Hamilton, A., Jenkins, J., Jones, R., King, B., Kolus, H., Larsen, J., Levin, A., Mahajan, M., Marcy, C., Mayfield, E., McFarland, J., McJeon, H., … Zhao, A. (2023). Emissions and energy impacts of the Inflation Reduction Act. *Science*, *380*(6652), 1324–1327. https://doi.org/10.1126/science.adg3781

Burton, D. (2023, March 20). *The Solar + Wind Finance and Investment Summit Soundbites: the Tax Equity Market and Transferability*. Norton Rose Fulbright: Project Finance.Brown, T. (2022, April 22). *Prices for California's emissions credits increase in early 2022 auction*.

Campion, N., Nami, H., Swisher, P., Hendriksen, P. V., & Münster, M. (2022). Techno-Economic Assessment of Green Ammonia Production with Different Wind and Solar Potentials. *Social Science Research Network*. https://doi.org/10.2139/ssrn.4154006

Cole, W. J., & Frazier, A. (2019). *Cost Projections for Utility-Scale Battery Storage*. https://doi.org/10.2172/1529218

Cheema, I. I., & Krewer, U. (2018). Operating envelope of Haber–Bosch process design for power-to-ammonia. *RSC Advances*, *8*(61), 34926–34936. https://doi.org/10.1039/c8ra06821f

Cocon, Kamyll Dawn. *Towards an agile Power-to-Ammonia pathway : optimization of a dynamic ammonia production process*. Ecole polytechnique de Louvain, Université catholique de Louvain, 2021. Prom. : Contino, Francesco.

Cybulsky, A., Giovanniello, M., Schittekatte, T., & Mallapragada, D. S. (2023). Producing hydrogen from electricity: How modeling additionality drives the emissions impact of time-matching requirements (MITEI-WP-2023-02).

Davenne, T., Huddart, A., Cowan, R., Tallentire, D., Peters, B., Smith, J., Ruddell, A., & Halliday, J., Ammonia Synthesis Plant from Intermittent Renewable Energy (ASPIRE). Frazer-Nash Consultancy. https://assets.publishing.service.gov.uk/government/uploads/system/uploads/attachment_data/file/1158095/HYS2169_STFC_Final_Feasibility_Report__Confidential___Public_.pdf

Damodaran, A. (2023, January). *Cost of Equity and Capital (US)*.

Dimanchev, E., Fleten, S., MacKenzie, D., & Korpas, M. (2023). Accelerating Electric Vehicle Charging Investments: A Real Options Approach to Policy Design. *Energy Policy*, *181*.

Dincer I. and Ishaq H. (2021) Renewable Hydrogen Production, Elsevier, Amsterdam, Netherlands.

Dunning, Mitchell, & Sullivan. (2011). PuLP : A Linear Programming Toolkit for Python. *Semantic Scholar*. https://www.semanticscholar.org/paper/PuLP-%3A-A-Linear-Programming-Toolkit-for-Python-Mitchell-O%27Sullivan/24c9ad0d66f6a05ad41563a7dade60bff6f59106

dos Santos, K. G., Eckert, C. T., de Rossi, E., Bariccatti, R. A., Frigo, E. P., Frigo, E. P., Lindino, C. A., Lindino, C. A., & Alves, H. J. (2017). Hydrogen production in the electrolysis of water in Brazil, a review. *Renewable & Sustainable Energy Reviews*. https://doi.org/10.1016/j.rser.2016.09.128

del Pozo, C. A., & Cloete, S. (2022). Techno-economic assessment of blue and green ammonia as energy carriers in a low-carbon future. *Energy Conversion and Management*. https://doi.org/10.1016/j.enconman.2022.115312

Environmental Protection Agency (EPA). (2022). *Supplementary Material for the Regulatory Impact Analysis for the Supplemental Proposed Rulemaking, "Standards of Performance for New, Reconstructed, and Modified Sources and Emissions Guidelines for Existing Sources: Oil and Natural Gas Sector Climate Review."*

European Commission. (2023). *Carbon Border Adjustment Mechanism*.

Energy Information Administration (EIA). (2023a). *Annual Energy Outlook 2023*.

EIA. (2023b, June). *Natural Gas Spot and Futures Prices (NYMEX)*.

Gilbert, P., Alexander, S., Thornley, P., & Brammer, J. (2014). Assessing economically viable carbon reductions for the production of ammonia from biomass gasification. *Journal of Cleaner Production*. https://doi.org/10.1016/j.jclepro.2013.09.011

Gomez, J., Baca, J. M., Garzon, F. H., & Garzon, F. H. (2020). Techno-economic analysis and life cycle assessment for electrochemical ammonia production using proton conducting membrane. *International Journal of Hydrogen Energy*. https://doi.org/10.1016/j.ijhydene.2019.10.174

Guerra, C. F., Reyes-Bozo, L., Vyhmeister, E., Caparrós, M. J., Salazar, J. L., Salazar, J. L., & Clemente-Jul, C. (2020). Technical-economic analysis for a green ammonia production plant in Chile and its subsequent transport to Japan. *Renewable Energy*. https://doi.org/10.1016/j.renene.2020.05.041

D. Green and M. Southard (2018), Perry's Chemical Engineers Handbook, 9th Edition, McGraw Hill, NY.

Herzog, H. J. (2011). Scaling up carbon dioxide capture and storage: From megatons to gigatons. *Energy Economics*, *33*(4), 597–604. https://doi.org/10.1016/j.eneco.2010.11.004

Inflation Reduction Act (IRA), Pub. L. No.117-169, 136 Stat. 1818 (2022)

International Energy Agency (IEA). (2021). *Ammonia Technology Roadmap Towards more sustainable nitrogen fertilizer production*. www.iea.org/t&c/

IEAGHG. (2017). *Techno-Economic Evaluation fo SMR Base Standalone (Merchant) Plant with CCS*.

International Renewable Energy Agency (IRENA). (2020). Green Hydrogen Cost Reduction - Scaling up electrolysers to meet the 1.5C climate goal. In *International Renewable Energy Agency*.

IRENA, & Ammonia Energy Association (AEA). (2022). Innovation Outlook: Renewable Ammonia.

Jenkins, J., & Ricks, W. (2023). *The Cost of Clean Hydrogen with Robust Emissions Standards: A Comparison Across Studies*.

Kakoulaki, G., Kougias, I., Taylor, N., Dolci, F., Moya, J., & Jäger-Waldau, A. (2021). Green hydrogen in Europe – A regional assessment: Substituting existing production with electrolysis powered by renewables. *Energy Conversion and Management*, *228*. https://doi.org/10.1016/j.enconman.2020.113649

Lazouski, N., Limaye, A., Bose, A., Gala, M. L., Manthiram, K., & Mallapragada, D. S. (2022). Cost and performance targets for fully electrochemical ammonia production under Flexible Operation. *ACS Energy Letters*, *7*(8), 2627–2633. https://doi.org/10.1021/acsenergylett.2c01197

Lee, B., Lim, D., Lee, H., & Lim, H. (2021). Which water electrolysis technology is appropriate?: Critical insights of potential water electrolysis for green ammonia production. *Renewable & Sustainable Energy Reviews*. https://doi.org/10.1016/j.rser.2021.110963

Liu, X., Elgowainy, A., Wang, M., & Wang, M. (2020). Life cycle energy use and greenhouse gas emissions of ammonia production from renewable resources and industrial by-products. *Green Chemistry*. https://doi.org/10.1039/d0gc02301a

Martin, K. (2021, February 18). *Tax credits for carbon capture*. Norton Rose Fulbright: Project Finance.

Maxwell, G. R. (2012). *Synthetic Nitrogen Products*. https://doi.org/10.1007/978-1-4614-4259-2_22

MacFarlane, D. R., Cherepanov, P. V, Choi, J., Suryanto, B. H. R., Hodgetts, R. Y., Bakker, J. M., Ferrero Vallana, F. M., & Simonov, A. N. (2020). A Roadmap to the Ammonia Economy. *Joule*, *4*(6), 1186–1205. https://doi.org/https://doi.org/10.1016/j.joule.2020.04.004

McDonald, J. (2023, February 8). CBAM, ETS reform to impact fertilizer trade. *S&P Global Commodity Insights*.

Nicholson, S., & Heath, G. (2021). Life Cycle Emissions Factors for Electricity Generation Technologies.

Lewis, E., McNaul, S., Jamieson, M., Henriksen, M., Matthews, H. S., Walsh, L., Grove, J., Shultz, T., & Stevens, R. (2022). Comparison of Commercial, State-of-the-Art, Fossil-Based Hydrogen Production Technologies. *Null*. https://doi.org/10.2172/1862910

Onodera, H., Delage, R., & Nakata, T. (2023). Systematic effects of flexible power-to-X operation in a renewable energy system - A case study from Japan. *Energy Conversion and Management: X*, *20*, 100416. https://doi.org/10.1016/j.ecmx.2023.100416

Ostuni, R, & Zardi, F. (2011). Method for load regulation of an ammonia plant (U.S. Patent No. 9463983B2). U.S. Patent and Trademark Office. https://rb.gy/ik0fb0

O'Donoughue, P. R.; Heath, G. A.; Dolan, S. L.; Vorum, M. (2014). Life Cycle Greenhouse Gas Emissions of Electricity Generated from Conventionally Produced Natural Gas*. Journal of Industrial Ecology, 18(1), 125–144.* doi:10.1111/jiec.12084

Open Energy Data Initiative (OEDI). (2022). OEDI: 2022 Annual Technology Baseline (ATB) Cost and Performance Data for Electricity Generation Technologies. Data Energy .

Osman, O., Sgouridis, S., & Sleptchenko, A. (2020a). Scaling the production of renewable ammonia: A techno-economic optimization applied in regions with high insolation. *Journal of Cleaner Production*. https://doi.org/10.1016/j.jclepro.2020.121627

Pfenninger, S;Staffell, I. (2016). Long-term patterns of European PV output using 30 years of validated hourly reanalysis and satellite data. Energy 114, pp. 1251-1265. https://dx.doi.org/10.1016/j.energy.2016.08.060

Pfromm, P. H. (2017). Towards sustainable agriculture: Fossil-free ammonia. *Journal of Renewable and Sustainable Energy*. https://doi.org/10.1063/1.4985090

Peters, M. S., Timmerhaus, K. D., & West, R. E. (2003). Plant Design and Economics for Chemical Engineers 5th Edition. In *Journal of Petrology* (Vol. 369, Issue 1).

Proost, J. (2017). State-of-the-art CAPEX data for water electrolyzers, and their impact on renewable hydrogen price settings. *International Journal of Hydrogen Energy*. https://doi.org/10.1016/j.ijhydene.2018.07.164

Sánchez, A., Martín, M., & Vega, P. (2019). Biomass Based Sustainable Ammonia Production: Digestion vs Gasification. *ACS Sustainable Chemistry & Engineering*. https://doi.org/10.1021/acssuschemeng.9b01158

Singh, S. P., Ku, A. Y., Macdowell, N., & Cao, C. (2022). Profitability and the use of flexible CO2 capture and storage (CCS) in the transition to decarbonized electricity systems. *International Journal of Greenhouse Gas Control*, *120*, 103767. https://doi.org/10.1016/J.IJGGC.2022.103767

Simons, A. M., Simons, A., & Bauer, C. (2011). Life cycle assessment of hydrogen production. *Transition to hydrogen. Pathways toward clean transportation*. https://doi.org/10.1017/cbo9781139018036.006

Spath, P., Aden, A., Eggeman, T., Ringer, M., Wallace, B., & Jechura, J. (2005). Biomass to Hydrogen Production Detailed Design and Economics Utilizing the Battelle Columbus Laboratory Indirectly-Heated Gasifier. https://doi.org/10.2172/15016221

Schmidt, O., Gambhir, A., Staffell, I., Hawkes, A., Nelson, J., & Few, S. (2017). Future cost and performance of water electrolysis: An expert elicitation study. *International Journal of Hydrogen Energy*. https://doi.org/10.1016/j.ijhydene.2017.10.045

Scott, V., Gilfillan, S., Markusson, N., Chalmers, H., & Haszeldine, R. S. (2013). Last chance for carbon capture and storage. *Nature Climate Change*, *3*(2), 105–111. https://doi.org/10.1038/nclimate1695

Sousa, J., Waiblinger, W., & Friedrich, K. A. (2022). Techno-economic Study of an Electrolysis-Based Green Ammonia Production Plant. *Industrial & Engineering Chemistry Research*. https://doi.org/10.1021/acs.iecr.2c00383

Stehly, T., Beiter, P., & Duffy, P. (2020). *2019 Cost of Wind Energy Review*. https://doi.org/10.2172/1756710

Reiner, D. M. (2016). Learning through a portfolio of carbon capture and storage demonstration projects. *Nature Energy*, *1*(1), 15011. https://doi.org/10.1038/nenergy.2015.11

Ricks, W., Xu, Q., & Jenkins, J. D. (2023). Minimizing emissions from grid-based hydrogen production in the United States. *Environmental Research Letters*, *18*(1). https://doi.org/10.1088/1748-9326/acacb5

Riley, B. P., Daoutidis, P., & Zhang, Q. (2023). Multi-scenario design of ammonia-based energy storage systems for use as non-wires alternatives. *Journal of Energy Storage*, *73*, 108795. https://doi.org/10.1016/j.est.2023.108795

Rouwenhorst, K. H. R., Van der Ham, A. G. J., Mul, G., & Kersten, S. R. A. (2019). Islanded ammonia power systems: Technology review & conceptual process design. In *Renewable and Sustainable Energy Reviews* (Vol. 114). Elsevier Ltd. https://doi.org/10.1016/j.rser.2019.109339

Rouwenhorst, K. (2023, June 28). *China: Scaling-up "flexible" ammonia production powered by Renewable Energy*. Ammonia Energy Association. https://www.ammoniaenergy.org/articles/china-scaling-up-flexible-ammonia-production-powered-by-renewable-energy/#:~:text=Flexible%20ammonia%20production%20allows%20the,Skovgaard%20Energy%2C%20Vestas%20and%20Topse.

Ruhnau, O., & Schiele, J. (2023). Flexible green hydrogen: The effect of relaxing simultaneity requirements on project design, economics, and power sector emissions. *Energy Policy*, *182*, 113763. https://doi.org/10.1016/j.enpol.2023.113763

Tock, L., Maréchal, F., & Perrenoud, M. (2015). Thermo-environomic evaluation of the ammonia production. *The Canadian Journal of Chemical Engineering*. https://doi.org/10.1002/cjce.22126

Tunå, P., Hulteberg, C., & Ahlgren, S. (2014). Techno-economic assessment of nonfossil ammonia production. *Environmental Progress*. https://doi.org/10.1002/ep.11886

The Engineering ToolBox (2003). *Fuels - Higher and Lower Calorific Values*. [online] Available at: https://www.engineeringtoolbox.com/fuels-higher-calorific-values-d_169.html

Turton, R., Shaeiwitz, J., Bhattacharyya, D., & Whiting, W. (2018). *Analysis, Synthesis, and Design of Chemical Processes* (5th ed.). Prentice Hall.

Valente, A., Iribarren, D., & Dufour, J. (2020). Prospective carbon footprint comparison of hydrogen options. *Science of The Total Environment*. https://doi.org/10.1016/j.scitotenv.2020.138212

Vargas, M., McNutt, K., Seiple, C., & Mackenzie, W. (2023). Annual Matching Requirements For New IRA Tax Credits Could Kick-Start Economically Competitive Green Hydrogen Production. *Forbes*.

Verleysen, K., Parente, A., & Contino, F. (2023). How does a resilient, flexible ammonia process look? Robust design optimization of a Haber-Bosch process with optimal dynamic control powered by wind. *Proceedings of the Combustion Institute*, *39*(4). https://doi.org/10.1016/j.proci.2022.06.027

Wang, C., Walsh, S. D. C., Longden, T., Palmer, G., Lutalo, I., & Dargaville, R. (2022). Optimising renewable generation configurations of off-grid green ammonia production systems considering Haber-Bosch flexibility. *Energy Conversion and Management*, *280*, 116790. https://doi.org/10.1016/j.enconman.2023.116790

Wang, G., Mitsos, A., & Marquardt, W. (2020). Renewable production of ammonia and nitric acid. *Aiche Journal*. https://doi.org/10.1002/aic.16947

Young, A. F., Young, A. F., Villardi, H. G. D., Villardi, H. G. D., Araújo, L. S., Raptopoulos, L. S. C., & Dutra, M. S. (2021). Detailed Design and Economic Evaluation of a Cryogenic Air Separation Unit with Recent Literature Solutions. *Industrial & Engineering Chemistry Research*. https://doi.org/10.1021/acs.iecr.1c02818

Young, B., Krynock, M., Carlson, D. R., Hawkins, T., Hawkins, T., Hawkins, T. R., Marriott, J., Morelli, B., Jamieson, M., Jamieson, M., Cooney, G., Cooney, G., Skone, T. J., Skone, T. J., & Skone, T. J. (2019). Comparative environmental life cycle assessment of carbon capture for petroleum refining, ammonia production, and thermoelectric power generation in the United States. *International Journal of Greenhouse Gas Control*. https://doi.org/10.1016/j.ijggc.2019.102821

Young, T. M., Ostermeier, D., Thomas, J. D., & Brooks, R. T. (1991). The economic availability of woody biomass for the southeastern United States. *Bioresource Technology*. https://doi.org/10.1016/0960-8524(91)90106-t

Zhang, H., Zhang, H., Wang, L., herle, J. Van, Maréchal, F., & Desideri, U. (2020). Techno-economic comparison of green ammonia production processes. *Applied Energy*. https://doi.org/10.1016/j.apenergy.2019.114135